August 2023 | Volume 111 | Number 8

Proceedings OF THE IEEE

Coexistence and Spectrum Sharing Above 100 GHz

Circuits and Antennas Incorporating Gallium-Based Liquid Metal

Microwave Metalens Antennas

Point of View: Rethink Physical Security: Protecting Vehicles via Battery-Enabled Sensing and Control

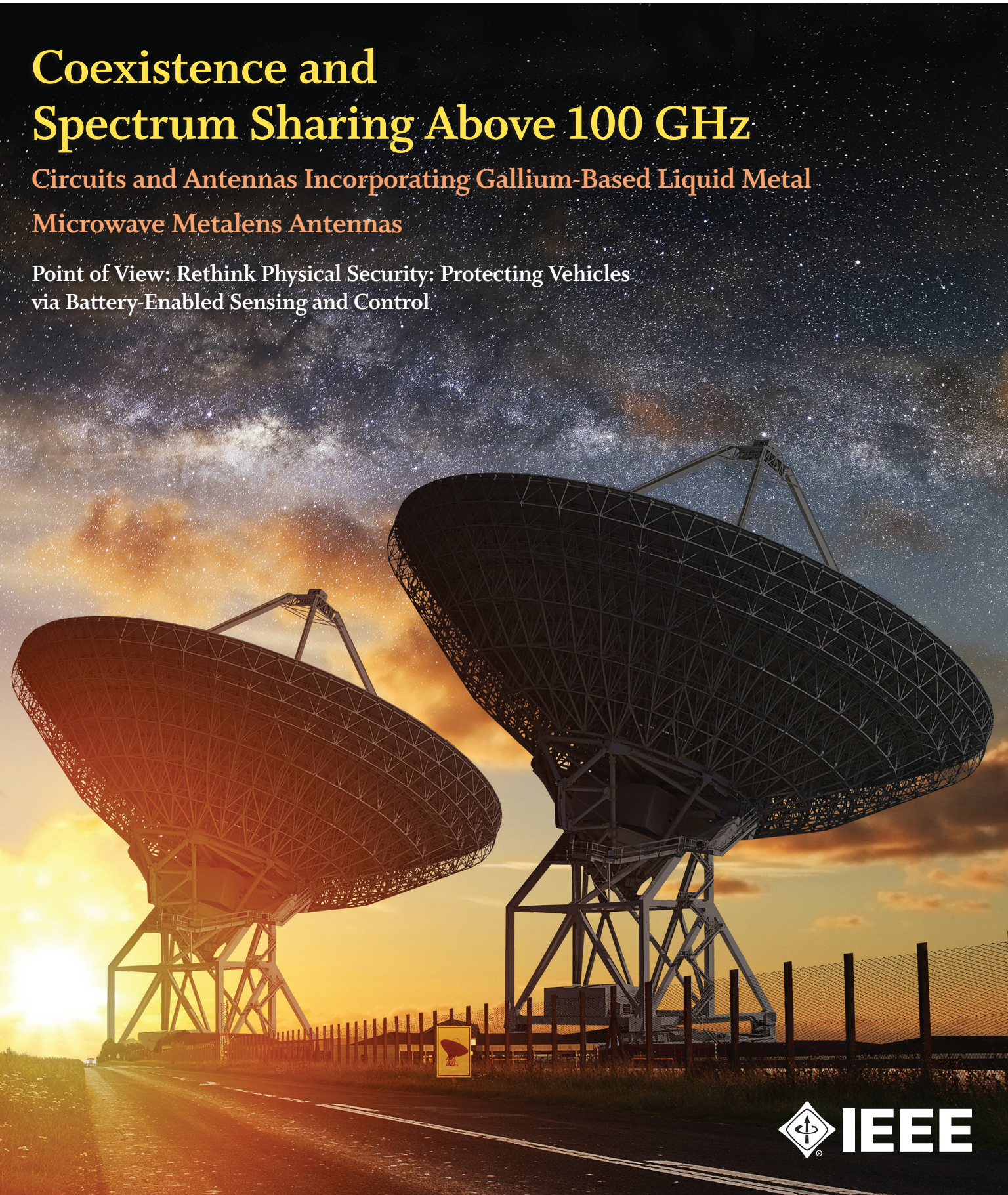

IEEE

CONTRIBUTED PAPER

Coexistence and Spectrum Sharing Above 100 GHz

This article provides policy and technological guidance on how sharing can be effectively implemented for the benefit of all the stakeholders in the spectrum above 100 GHz.

By Michele Polese, *Member IEEE*, Xavier Cantos-Roman, *Graduate Student Member IEEE*, Arjun Singh, *Member IEEE*, Michael J. Marcus, *Life Fellow IEEE*, Thomas J. Maccarone, Tommaso Melodia, *Fellow IEEE*, and Josep Miquel Jornet, *Senior Member IEEE*

ABSTRACT | The electromagnetic spectrum plays a fundamental role in the development of the digital society. It enables wireless communications (either between humans or machines) and sensing (for example, for Earth exploration, radio astronomy, imaging, and radars). While each of these uses benefits from a larger bandwidth, the spectrum is a finite resource. This introduces competing interests among the different stakeholders of the spectrum, which have led—so far—to rigid policies and spectrum allocations. Recently, the spectrum crunch in the sub-6-GHz bands has prompted communication technologies to move to higher carrier frequencies, where future sixth-generation (6G) wireless networks can exploit theoretically very large bandwidths. However, the spectrum above 100 GHz features several narrow, yet numerous subbands that are exclusively allocated for passive sensing applications, e.g., for climate and weather monitoring. This prevents the allocation of large contiguous bands to active users of the spectrum, either being communications (which need tens of gigahertz of bandwidth to target terabit-per-second links) or radars. This article explores how spectrum policy and spectrum technologies can evolve to enable *sharing* among different stakeholders in the above 100-GHz spectrum, without introducing harmful interference or disrupting either security applications or fundamental science exploration. This portion of the spectrum presents new challenges and opportunities for the design of spectrum sharing schemes, including higher spreading and absorption losses, extremely directional antenna technologies, and ultrahigh data-rate communications, among others. This article provides a tutorial on current regulations above 100 GHz and highlights how sharing is central to allowing each stakeholder to make the most out of this spectrum. It then defines—through detailed simulations based on standard International Telecommunications Union (ITU) channel and antenna models—scenarios in which active users may introduce harmful interference to passive sensing. Based on this evaluation, it reviews a number of promising techniques that can enable active/passive sharing above 100 GHz. The critical review and tutorial on policy and technologies of this article have the potential to kickstart future research and regulations that promote safe coexistence between active and passive users above 100 GHz, further benefiting the development of digital technologies and scientific exploration.

KEYWORDS | Coexistence; passive users; sixth generation (6G); spectrum sharing; submillimeter waves; terahertz communication.

Manuscript received 28 October 2021; revised 23 December 2022 and 25 March 2023; accepted 6 June 2023. Date of publication 3 July 2023; date of current version 26 July 2023. This work was supported in part by NSF under Grant AST-2037896, Grant MPS-2037890, Grant CNS-2011411, and Grant CNS-2225590. *(Corresponding author: Michele Polese.)*

Michele Polese, **Xavier Cantos-Roman**, **Michael J. Marcus**, **Tommaso Melodia**, and **Josep Miquel Jornet** are with the Institute for the Wireless Internet of Things and the Department of Electrical and Computer Engineering, Northeastern University, Boston, MA 02115 USA (e-mail: michele.polese@gmail.com).

Arjun Singh is with the Department of Engineering, State University of New York Polytechnic Institute, Utica, NY 13502 USA.

Thomas J. Maccarone is with the Department of Physics and Astronomy, Texas Tech University, Lubbock, TX 79409 USA.

Digital Object Identifier 10.1109/JPROC.2023.3286172

I. INTRODUCTION

The digital society of the next decade will increasingly rely on services provided by a fundamental, invisible, yet scarce resource, i.e., the electromagnetic spectrum. The wireless spectrum enables a diverse set of applications, from high-speed communications [1] to imaging [2], remote sensing [3], Earth and space exploration [4], and radio astronomy [5]. The radio frequency (RF) technologies, either communications or sensing, generally benefit from using a larger bandwidth, with a proportional improvement to the capacity and/or the sensing resolution [6], [7]. The finite nature of the spectrum,

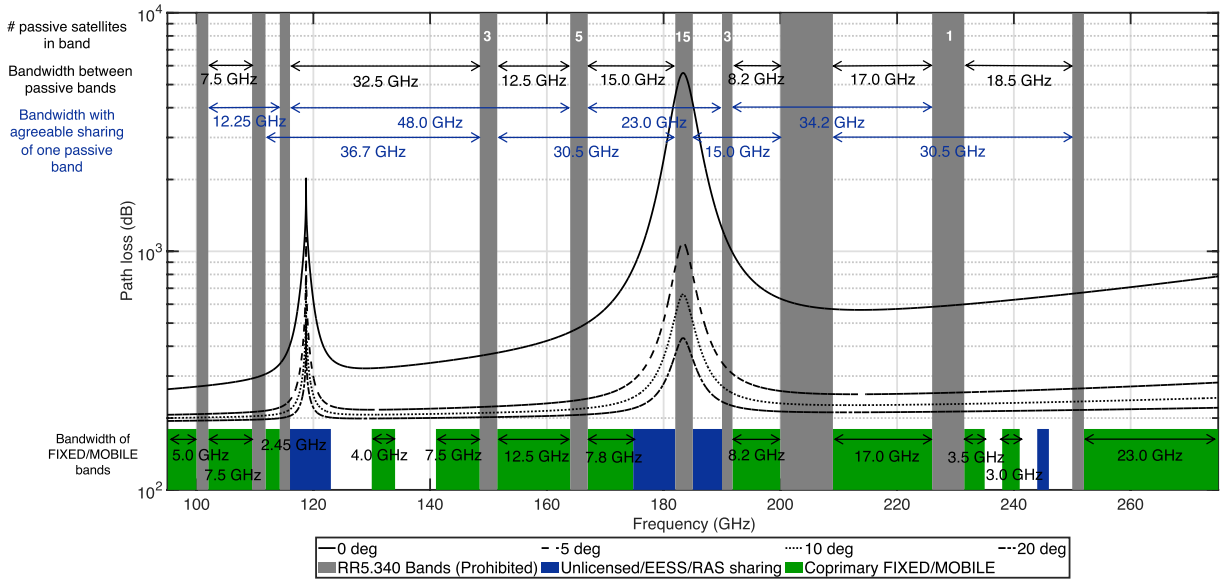

Fig. 1. ***Spectrum allocation above 100 GHz and the path loss for a 407-km Earth–space link with different elevation angles based on the channel model discussed in Section IV. The figure also describes existing services and spectrum allocation based on the International Telecommunications Union (ITU) radio regulations [18] and includes the number of passive satellites in each band dedicated to passive sensing. Finally, the top part of the figure reports the chunks of bandwidth, which are available between passive bands (black) or by enabling sharing of one passive band (blue).***

however, translates into limited availability of resources for each use case, prompting researchers to expand into new, unexplored portions of the spectrum, and to investigate sharing mechanisms. Notably, the crowded spectrum in the traditional sub-6 gigahertz (GHz) band has led fifth-generation (5G) networks, radars, and sensing systems to use the lower millimeter-wave (mmWave) band. For example, 3rd Generation Partnership Project (3GPP) NR, a 5G technology, is expected to use carrier frequencies as high as 71 GHz [8], while radars generally operate in multi-GHz bands around 60 and 77 GHz [9]. Similarly, policies and technologies have evolved to accommodate shared uses of the spectrum [10].

As the design and engineering of antennas and RF circuitry for high-frequency transceivers and sensors have improved, the spectrum above 100 GHz has entered the spotlight as an enabler of sixth-generation (6G) communications technologies, on the one side [11], and more advanced sensing solutions, on the other [12]. This portion of the spectrum includes large chunks of unused bandwidth, which both sensing and communications can benefit from.

Notably, certain sensing techniques integrate a large number of observations over time and frequency. As per the central limit theorem, the accuracy of the measurement is proportional to the square root of the number of observations [5]. Given a certain noise level target, a larger bandwidth allows measurements to be collected in a shorter time period, which is particularly beneficial in the case of dynamic sources or measurement setups. Similarly, radars can provide more precise tracking with a larger bandwidth [13]. In addition, the spectrum above 100 GHz features specific subbands of interest to the scientific community because of molecular transitions [4], [14]. Finally, larger bandwidth enables higher data rates for communications, with tens of GHz needed to target the terabit-per-second (Tb/s) data rate goal of future 6G networks [15], [16], as we discuss later in this article. The need for ultrahigh data rates is also shared by the scientific community to overcome limitations introduced by low-capacity telemetry links between sensing satellites in space and ground stations [17].

A. Sharing the Spectrum in the 21st Century

As a consequence, both sensing and communications communities have a stake in the spectrum above 100 GHz, either because of the availability of large chunks of untapped bandwidth or because of specific frequencies of interest. The different communities, however, often express different needs with respect to how the spectrum should be used. For example, even modest levels of radio frequency interference (RFI) can strongly affect the performance of most classes of passive sensing systems [19], while communications or other sensing techniques (e.g., some radars) need active transmissions. This has led national and international spectrum regulation entities to define a rigid allocation scheme in the spectrum above 100 GHz, with a set of narrow, yet numerous subbands exclusively dedicated to passive sensing (i.e., for science and space exploration) [18]. While the total bandwidth reserved for passive users is rather small (i.e., 33.35 GHz between 100 and 275 GHz), the positioning of these subbands in the overall spectrum prevents the allocation of large chunks of contiguous bandwidth for active usage. As highlighted in Fig. 1, the largest contiguous chunk allocated to active users between 100 and 275 GHz has

a bandwidth of 32.5 GHz (between 116 and 148.5 GHz). However, in this band, only 12.25 GHz (noncontiguous) are allocated to fixed and mobile communications (i.e., 122.25–123, 130–134, and 141–148.5 GHz), and the remaining 19.5 GHz are earmarked for active sensing techniques, radionavigation, and radiolocation. For communications, this is less than the bandwidth that is typically needed to achieve the 1-Tb/s target rate of future 6G networks. Similarly, the needs of the sensing community have evolved since when the current regulatory approach was established. At that time, the electronics for sensing systems were severely limited in terms of the bandwidth that they could handle, and millimeter-band astronomy facilities were not sensitive enough to see molecular features at large distances, where the expansion of the universe changes their wavelengths substantially. All of these aspects of the situation have now changed so that the current approach of protecting narrowbands everywhere all the time is no longer as valuable as protecting broader bands at specific places and times.

Therefore, a dynamic and shared use of the spectrum above 100 GHz will simultaneously enable next-generation sensing *and* communication technologies. Spectrum sharing has proven a successful enabler of advanced spectrum usage in the sub-6-GHz and lower mmWaves bands. A notable example is that of the Citizen Broadband Radio Service (CBRS) band, i.e., 150 MHz between 3.55 and 3.7 GHz, which have been repurposed for shared usage between sensing systems (e.g., U.S. Navy radars), critical communications (to and from aircrafts), and commercial users [20], [21]. According to the recent regulations for CBRS, secondary users (generally, commercial ones) need to preempt spectrum usage and effectively avoid RFI to the primary users. This shows that it is possible to go beyond a strict resource partitioning scheme with exclusive spectrum access, with a mutually beneficial outcome, i.e., more bandwidth can be *dynamically* allocated to different services according to need. Along this line, a National Research Council report [22] shows that—with proper coordination—a constellation of 30 sensing satellites and active users on the ground can share the same bands with active transmissions for 99.7% of the time and without any interference to the passive sensing system. The ITU has also advanced a resolution at the World Radio Conference (WRC) in 2000 to promote sharing of the passive bands above 71 GHz, as long as sharing does not expose passive services to interference levels beyond those standardized by ITU [23], [24], [25], [26].

The characteristics of devices and propagation in the above 100 GHz introduce new opportunities and challenges with respect to spectrum sharing approaches in the sub-6-GHz band [27], considering approaches that are based on device design, the signal processing at the physical layer, and coordination at the medium access control (MAC) and above. The higher spreading and absorption losses above 100 GHz [11], together with directional transceiver architectures [28], allow for increased spatial reuse and coexistence. Similarly, a larger bandwidth can shorten the observation time for sensing and the transmission time for communications, thus potentially enabling more refined and flexible time-sharing strategies. At the same time, however, the device and RF circuit design is made more challenging by the high carrier frequency and large-bandwidth processing requirements. This complicates the design of precise transmit and receive frequency masks, leading to out-of-band emission issues. In addition, the extreme directionality required to close the link in this portion of the spectrum introduces a deafness problem, which complicates the design of sensing- and beaconing-based sharing even when compared to mmWave frequencies.

B. Contributions and Article Structure

The implementation of spectrum sharing techniques, therefore, requires a concerted effort involving the different stakeholders of the spectrum above 100 GHz and innovations in both spectrum policy and engineering. This article represents a critical step to make this portion of the spectrum ready for the technologies that will use it in the future, replacing a set of regulations that date back to the 1930s [29], [30].

This article provides policy and technological guidance on how sharing can be effectively implemented for the benefit of all the stakeholders in the spectrum above 100 GHz, enabling the digital revolution of the next decade. Notably, it is the first paper that does the following.

1) It describes the needs of the stakeholders in the spectrum above 100 GHz, detailing—with numerical examples—why both sensing and communications can benefit from access to large, contiguous chunks of bandwidth in this portion of the spectrum.
2) It provides a detailed description of the current spectrum regulations in this band, highlighting possible policy roadblocks that prevent dynamic spectrum sharing between different stakeholders.
3) It adopts a physics-based approach to model the interference between active systems and passive users, to understand which scenarios and operating regimes are subject to RFI in the spectrum above 100 GHz. The modeling will consider realistic settings and conditions, i.e., high-sensitivity receivers for the sensing systems and directional antenna arrays in the communication systems, and will be based on ITU channel models and antenna patterns. Our analysis highlights that, while the high path loss and directional antennas can help reduce RFI in some scenarios, there are configurations (e.g., for high satellite elevation angles) where RFI from terrestrial communications links exceeds the harmful RFI thresholds for passive services set by the ITU.
4) It analyzes technological enablers of spectrum sharing in the spectrum above 100 GHz, considering established techniques (e.g., signal processing for

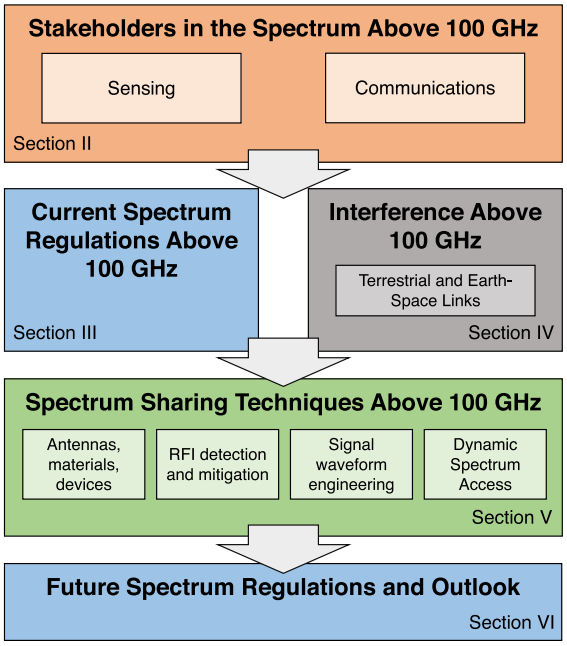

Fig. 2. ***Structure of this article.***

RFI mitigation), specific solutions at higher frequencies (e.g., metasurfaces and extremely directional arrays), and research directions and challenges toward spectrum sharing above 100 GHz. We review full-stack solutions, i.e., hardware-based RFI mitigation (innovative antenna design, antenna arrays, and frequency-selective surfaces (FSSs)), signal processing, and communications and networking design.

5) It discusses how spectrum regulations and technologies can evolve to accommodate more shared spectrum, proposing future directions for technology and policy development, experimentation, and commercialization of sensing and communications solutions above 100 GHz.

The remainder of this article is organized as follows (see Fig. 2). Section II describes why the spectrum above 100 GHz is of interest for both the sensing and communication communities, and why more bandwidth is generally useful for both. Section III outlines the current regulations that prevent a flexible use of the spectrum above 100 GHz, while Section IV presents numerical results on the interference that can arise in different scenarios. Based on this analysis, Section V introduces and reviews possible spectrum sharing techniques and related research challenges. Finally, Section VI concludes this article with a discussion on what is required to enable spectrum sharing above 100 GHz.

II. STAKEHOLDERS IN THE SPECTRUM ABOVE 100 GHz

As shown in Fig. 3, the spectrum above 100 GHz is an attractive resource for a diverse set of stakeholders. In the following, we will discuss why each user of the spectrum is interested in using a large bandwidth, focusing specifically on the spectrum above 100 GHz and providing a quantitative assessment when relevant.

A. Sensing

Sensing applications that require access to spectrum consist of three broad categories: radar systems, passive Earth-observing systems, and astronomy systems. Broadband (or continuum) and narrowband applications are both important in the Earth-observing and astronomical contexts.

The narrowband work focuses on the detection of specific molecules. Key molecules for atmospheric science include molecular oxygen (at 60 GHz) and water vapor (at 183 GHz). For astronomy, the most important molecule has traditionally been carbon monoxide (CO) (at 115, 230, and 346 GHz), which is the most abundant asymmetric molecule and, hence, the strongest emission feature from regions with dense gas.

Broad bandwidths can be desirable for molecular line astronomy. This is because of Doppler motions and general relativistic effects due to the expansion of the universe, which can have a significant impact by moving the sensing target out of typical narrowbands. With facilities that exist or are planned for the near future, the strongest molecular features may be detectable up to distances sufficiently close to the edge of the observable universe. In this case, their wavelengths may be a factor of about 4 larger as we observe them than the wavelengths of the same molecular transitions as measured in a laboratory. This makes the case for broadband access to the spectrum for radio astronomy sensing. In addition, the increasing sensing capabilities of modern scientific facilities have allowed observers in recent years to measure phenomena related to a much larger number of rare molecules, which span the whole electromagnetic spectrum. In general, projects that involve the characterization of the emission of a single known molecule can usually do well with narrowband observations, while projects that involve searches for new molecules typically need broadband access to the spectrum, even if the features to be observed are narrow ones.

Typical spectral widths of the features vary by application. Atmospheric features are susceptible to pressure

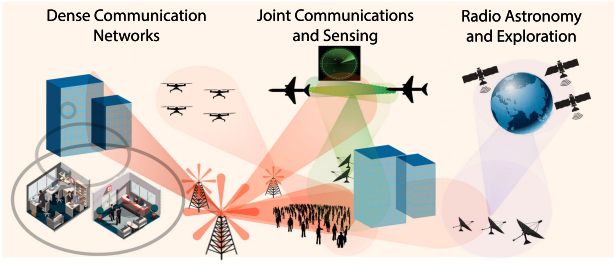

Fig. 3. ***Stakeholders in the spectrum above 100 GHz.***

broadening (i.e., the intrinsic energies of the transitions in one molecule can be affected by forces exerted from other molecules) and, sometimes, Zeeman broadening (i.e., they are broadened by forces from the Earth's magnetic field affecting the energy levels within molecules). In addition, some atmospheric molecular features come in bands with many adjacent transitions. The oxygen absorption band, for example, consists of a large set of absorption features, pressure broadened to create a smooth feature from about 50–70 GHz, and the water vapor band at 183 GHz also spans a fairly broad range, dominating atmospheric opacity from about 165 to 200 GHz [31]. Astronomical narrowband features typically have widths no more than those of the Doppler shifts associated with the orbital speeds of galaxies. These are typically ≈200–400 km/s, giving fractional widths of about 1/1000, or a few hundred MHz. There are, however, also often isotopic features adjacent to the primary molecular feature that astronomers wish to observe simultaneously with the primary feature. These have fractional separations about the same as the fractional mass difference between the dominant and rarer isotopes, so they are typically shifted by about 5% from the main feature for the light molecules that are most abundant (e.g., in addition to CO at 230 GHz, there are ^{13}CO at 220 GHz and C^{18}O at 210 GHz).

Finally, broadband passive work also focuses on the detection of thermal and synchrotron emission.[1] Broadband active sensing work largely involves the use of the millimeter band to do the same kind of work as lower frequency radars, taking advantage of the short wavelength at these frequencies to perform finer imaging. Broadband passive systems generally study phenomena with emission across the entire millimeter band, so the restrictions of sensing applications arise from the limitations on the receivers, and the electronics and computational processing systems. Currently, these generally impose 20% fractional bandwidths on the receivers and 8–50-GHz total bandwidth from the electronics. Nonetheless, technological improvements have consistently pushed these limits over the past few decades, and there are no indications that such progress is slowing down. The spectrum above 100 GHz is also used for some very short-range imaging applications (e.g., medical imaging and security scanners).

In the following, we will discuss in detail the use cases for narrowband and continuum sensing.

1) Narrowband Applications: The narrowband applications are largely driven by a particular set of frequencies for specific rotational transitions of molecules, largely within the 10–500-GHz range. Earth-sensing satellites and high-altitude airplanes can use these molecular features to map out quantities, such as the chemical composition of the atmosphere and cloud cover and humidity, among others [32], [33], [34]. Such measurements are important for both meteorology and climate science.

For astronomical objects, molecular features can provide information not just about chemical compositions but also temperatures and densities of regions in space. Temperatures are largely probed by the fraction of a single compound's molecules in different excited states, while densities and chemical compositions can then be inferred from the relative abundances of different molecules. In recent years, improvements in the sensitivity of astronomical facilities in the 10–500-GHz band have made it possible for astronomers to detect a wide range of new molecules [35]. The newest facilities can also detect molecules with the brightest features at distances where the expansion of the universe introduces large cosmological redshifts [36]; these large cosmological redshifts can also move important molecular transitions out of protected bands into unallocated frequency ranges. Both of these developments mean that even the portion of the passive sensing community working with narrow spectral features has *applications that span the full spectrum*.

2) Broadband (or Continuum) Sensing: There is considerable interest in moving automotive and other radar systems above 100 GHz although this work is still in relatively early stages of development [37], [38], as the larger bandwidth and shorter wavelength lead to better range, angular, and velocity resolutions. The range resolution ΔR of radar based on pulse compression depends on the bandwidth of the transmitted pulse, i.e.,

$$\Delta R = \frac{c}{2B} \tag{1}$$

where c is the speed of light and B is the bandwidth. The angular resolution depends on the antenna beamwidth, which is related to the electrical length and corresponding directivity of the antenna. The velocity resolution depends on the Doppler spectrum that is also related to the wavelength of the transmitted signal. Moreover, in some cases, the propagation challenges of working in the above 100-GHz band are a positive feature; a higher density of automotive radar systems can be tolerated if propagation losses keep the systems from interfering with one another over large distances.

Broadly speaking, however, the continuum work presently done in this band is radio astronomy. Continuum work in radio astronomy is usually done to look at cool thermal emitters, such as: 1) interstellar dust; 2) the disks around young stellar objects, in which planets form (which typically have temperatures of a few hundred Kelvin); or 3) the cosmic microwave background (which has a temperature of 2.7 K). It can also be used to look at sources of synchrotron emission at high frequencies. The highest angular resolution images that can be made by astronomers come from millimeter-band very long baseline interferometry, work done at 230 GHz [39]. At longer

[1]Synchrotron emission is the relativistic version of cyclotron emission and is produced when electrons with speeds very close to the speed of light produce radiation as they are accelerated by magnetic fields.

wavelengths, the angular resolution is insufficient to measure black hole shadows without space-based antennas (which currently lack the sensitivity to do so). At infrared bands, interferometry has only been possible with direct interference of signals from physically connected telescopes, limiting baselines to a few hundred meters. The millimeter band is the shortest wavelength on which data can be recorded and global baselines can be achieved. This capability allowed—for example—the measurement of the size of the shadow of a black hole event horizon in the galaxy M87 [39]. In most cases of continuum imaging, the largest possible bandwidth is desired in order to detect faint signals, but, for sufficiently bright sources, with sufficiently large bandwidths, the spectral shape of a source can be measured with a single observation at a single band.

The sensitivity of a radiometer is derived from the radiometer equation

$$\Delta T = \frac{T_{\text{sys}}}{\sqrt{B\tau}} \tag{2}$$

where ΔT is the residual (root-mean-square) uncertainty in a noise temperature measurement, T_{sys} is the noise temperature of the system being measured, and $B\tau$ is the product between bandwidth B and time τ of observation [40]. The signal-to-noise of a source is then derived from the ratio of the source brightness temperature, T_{source}, and ΔT. Notably, $T_{\text{source}} = (A_e/2k_B)S_\nu$, where A_e is the effective area of the system, k_B is Boltzmann's constant, and S_ν is the flux density of the source per angular resolution element.

Radio astronomy requires ultralow noise levels. Reaching these in short exposure times is always desirable, as, at a minimum, it enables a larger number of observations to be done. In addition, in some cases, strong source variability is the goal of the measurement itself [41], with the consequence that the measurement must be completed quickly in order to make reliable aperture synthesis images [39]. Increases in sensitivity in a given exposure time can be achieved either by increasing the bandwidth available or by increasing the effective area of the system. Bandwidth increases are generally preferred because electronics upgrades are usually much less expensive than adding antennas or increasing the sizes of the antennas used. Available bandwidth currently varies among the different telescopes. The receiver bands are generally limited to about 20% of the central frequency. At the present time, millimeter-band interferometers typically use about 8 GHz, with the specific frequencies chosen based on the science case for the user.[2,3] However, for the Atacama large millimeter array, planning is already underway to upgrade the correlators to allow at least a factor of 2 increase in bandwidth [42]. Single-dish radio telescopes have larger bandwidths; for example, the TolTEC instrument for the large millimeter telescope planned to reach about 60 GHz of bandwidth.[4] The present regulatory framework was established in an era long before the current tens of GHz of bandwidth systems were practical.

Currently, a rather limited number of radio astronomy facilities engage in sensing above 100 GHz. All such facilities are in high-altitude, dry locations, generally several kilometers or more from settled locations; the requirement of detecting faint signals mandates choosing sites with minimal propagation losses. A substantially larger (albeit still small) number of telescopes work in the 90-GHz band, and the CLOUDSAT satellites of NASA have successfully avoided interfering with them for 15 years. It should be straightforward to continue to avoid interference with ground-based scientific users.

B. Communications

Several early papers on 6G communication technologies have highlighted how the spectrum above 100 GHz could be a fundamental enabler of ultrahigh-capacity wireless networks [16], [27], [43]. Results and demonstration of the feasibility of communicating in the (sub)terahertz bands have also been shown in several works, for example, as in [44]. The main challenges for communications in this portion of the spectrum are associated with: 1) the sensitivity to blockage and the high propagation loss [11], which can be offset, however, using directional antennas; 2) the presence of frequency-selective fading in specific bands, which increases with the humidity; and 3) the engineering and manufacturing of embedded RF circuitry that can operate at such high frequencies [45]. Additional challenges are related to the interfacing with the higher layers of communications protocol stacks, such as neighbor and infrastructure discovery challenged by directional links, and processing data at ultrahigh rates [16].

Nonetheless, the need for Tb/s data rates in 6G networks makes a compelling use for the deployment of communication services in the spectrum above 100 GHz, with a vast available bandwidth. Indeed, the achievable data rates R of a wireless link (with an ideal, frequency-flat channel) are proportional to the bandwidth B, scaled by the spatial reuse or diversity factor K and the spectral efficiency S, and by a function $f(\cdot)$ of the link signal-to-interference plus noise ratio (SINR) Γ

$$R \propto K \cdot S \cdot B \cdot f(\Gamma) \tag{3}$$

where $f(\cdot)$ is a generic function expressing the relationship between SINR and achievable rate, and the different elements K, S, and B in (3) highlight how next-generation communication technologies can improve on existing ones

[2]https://almascience.eso.org/about-alma/alma-basics

[3]https://www.iram.fr/IRAMFR/GILDAS/doc/pdf/noema-intro.pdf

[4]http://toltec.astro.umass.edu

to increase the communication rates. Notably, higher spectral efficiency can be achieved through more spectrally efficient modulations, e.g., orthogonal frequency-division multiplexing (OFDM) and its variants [46], [47], [48], combined with high order quadrature amplitude modulation (QAM) (with 1024-QAM and even above). This is represented in (3) by the scaling factor $S = \log_2(M)$, with M being the modulation order. Spatial reuse and diversity can be achieved using multiple-input–multiple-output (MIMO) techniques, which allow multiple data streams to be transmitted over the same time and frequency resources. This is represented in (3) by the scaling factor K, which we model as the number of MIMO streams, proportional to the rank of the channel matrix. A recent MIMO evolution, i.e., massive MIMO [49], has been shown to improve the SINR term as well, by exploiting the much larger number of antennas at the transmitter as compared to the receiver. The idea of ultramassive MIMO (UM-MIMO) [50] extends this even further, by packing thousands of antenna elements in small, portable arrays. Small cells and ultradense networks also help increase the spatial reuse factor K, sometimes at the cost of increased interference that penalizes the term Γ. Similarly, increasing the communication bandwidth B allows for a linear increase in the product outside function $f(\cdot)$, but, at the same time, the noise term of the SINR Γ increases proportionally to B.

The data rate increase for 6G networks will be given by a combination of the elements above. Nonetheless, the bandwidth plays a key role, as we show in Fig. 4. Each bar in the figure represents the bandwidth required to achieve a data rate of $R_t = 1$ Tb/s, which is expected to be one of the defining key performance indicators (KPIs) of 6G networks [15], [51] for a number of applications, including backhaul [51], [52], [53], immersive, holograph-based virtual experience [54], data offloading in vehicular networks [55], and mobile hotspot scenarios [51]. Notably, the bandwidth is computed as the ratio between the target rate R_t and the efficiency η of the MIMO and modulation order in use, i.e., $\eta = \hat{K}\hat{S}/\alpha$, with $\hat{K}$ being the number of MIMO streams, $\hat{S}$ the bit per symbol rate of a certain modulation order, and $\alpha = 1$ for single-sided waveforms, 2 otherwise. Fig. 4(a) considers a configuration with massive MIMO capabilities and highlights how an extremely high number of MIMO channels, combined with a high modulation order, make it possible—in principle—to reach the data rate target with bandwidths that are comparable to those of current 5G systems. Designing and engineering a system with such capabilities, however, are not trivial. A large number of MIMO streams require a massive number of antennas, as well as diversity in the channel conditions, and this may not be always feasible, especially when considering point-to-point backhaul links or portable devices in the sub-6-GHz spectrum.

Portable arrays with hundreds of antenna elements are instead feasible above 100 GHz, thanks to the small wavelength that translates into small antenna elements [50].

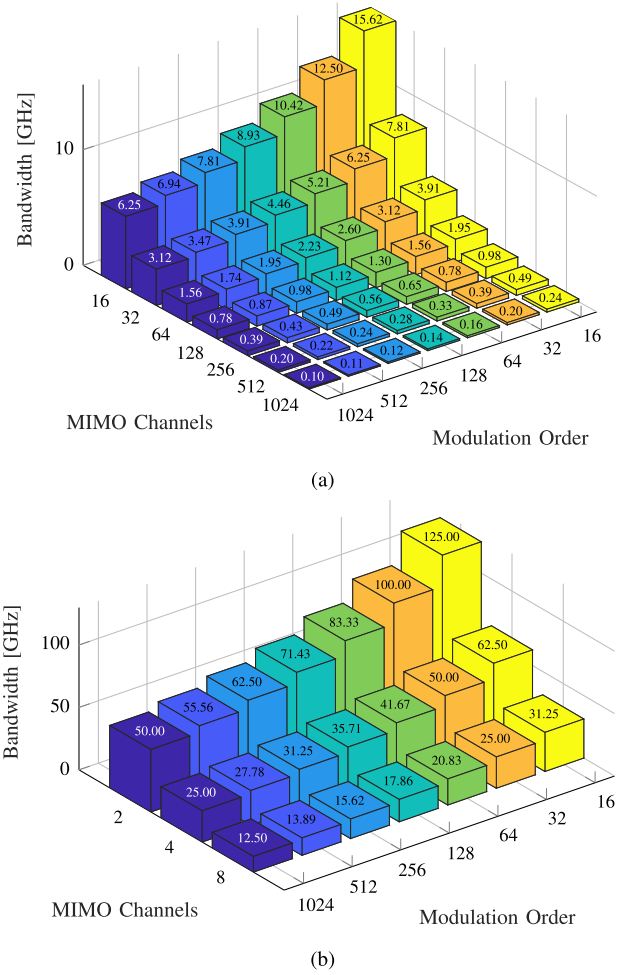

Fig. 4. ***Required bandwidth to achieve a 1-Tb/s data rate, as a function of modulation order and MIMO channels for OFDM. (a) High number of MIMO streams (e.g., enabled by massive MIMO). (b) Low number of MIMO streams.***

At such high frequencies, however, it becomes extremely complex to design multichannel and/or multiuser MIMO systems with a high number of channels. The state of the art of research on baseband design for such systems is represented by 4 × 4 and 8 × 8 MIMO systems [56], [57]. To this end, Fig. 4(b) considers configuration with a more practical number of parallel MIMO streams (i.e., up to 8). In this case, even with an OFDM modulation with 1024-QAM per channel, more than 12.5 GHz of contiguous bandwidth is needed.

In addition, such constellations often require extremely good channel conditions and low noise (both in amplitude and phase). Therefore, more practical configurations are represented on the right part of Fig. 4(b), with 16-QAM, which further increases the requirement in terms of bandwidth (i.e., 31.25 GHz with 16-QAM and 8 × 8 MIMO). Therefore, *the need for ultrawide bandwidth makes the spectrum above 100 GHz a key enabler for future 6G communications.*

Table 1 Bands Above 100 GHz With Mobile or Fixed Allocations Without Passive Allocations. Most of These Bands Have Coprimary Allocations With Other Active Services

Band (GHz)	122.25-130	158.5-164	167-174.8	191.8-200	231.5-235	238-241
Bandwidth (GHz)	7.5	5.5	7.8	8.2	3.5	3
Primary allocation	Fixed-Satellite/Mobile-Satellite	Fixed/Mobile	Fixed/Mobile	Fixed/Mobile	Fixed/Mobile	Fixed/Mobile

III. CURRENT SPECTRUM REGULATIONS ABOVE 100 GHz

Enabling sharing of the spectrum above 100 GHz will require both technological progress and policy updates. This section reviews the development of spectrum policy for the bands between 100 and 275 GHz (as there are no formal ITU allocations above 275 GHz yet), highlighting the roadblocks and opportunities toward a sharing-conscious spectrum policy. Notably, we review and summarize international regulations and provide a historical perspective on how they have been developed, together with a discussion on how the characteristics of the spectrum above 100 GHz have led to different policies when compared to sub-6-GHz or lower mmWave spectrum.

A. International Telecommunications Union

At the international level, the spectrum is regulated by the ITU, a United Nations agency with 193 member states that develop the ITU Radio Regulations (RR), a treaty document generally binding on its signatories. While these rules do not require countries to use spectrum in certain ways, they prohibit them from causing "harmful interference" to spectrum uses of other countries that are fully consistent with the rules. While most regulations involve active transmitters for applications such as telecommunications, broadcasting, and radar/radiolocation, the ITU also recognizes and protects passive scientific uses of the spectrum. As discussed in Section II, these use cases involve only the reception of naturally occurring emissions in specific spectrum bands, for example, for radio astronomy and environmental monitoring. Notably, the spectrum above 100 GHz features several bands that are reserved for the passive community. Table 1 and Fig. 1 list the bands with primary or coprimary fixed and/or mobile allocations, without any coprimary passive allocation[5]: in the present allocation scheme, the maximum fixed or mobile congruous bandwidth below 252 GHz is 8.2 GHz. This, as previously discussed, motivates the development of spectrum sharing solutions.

B. WRC-2000 and Spectrum Policy Above 100 GHz

Prior to the ITU WRC in 2000, ITU had few rules and allocations dealing with spectrum above 100 GHz. At that conference, similar proposals from both the United States and the European Conference of Postal and Telecommunications Administrations (CEPT) advocated the basic policies now in place in 100–275 GHz [58]. The policies advocated by the United States and Europe included both numerous passive allocations above 100 GHz, some bands with no passive allocations at all, and some bands in which active services and passive services could nominally share on a "coprimary" basis.

Ten passive-only bands were created in the 100–275-GHz spectrum, using the restriction in footnote 5.340 of the allocation table (also known as RR5.340) [18], previously used for lower frequency passive bands. The RR5.340 states that "all emissions are prohibited" in these bands, which cover 19% of the 100–275-GHz spectrum. Table 2 compares the amount of "prohibited" spectrum in the extremely high frequencies (EHF) band (30–300 GHz) with lower spectrum regions. While the amount of prohibited spectrum in ultrahigh frequencies (UHF) and super high frequencies (SHF) (below 30 GHz) is negligible, it covers 15% of the entire EHF region. In addition, the 15 protected bands in the EHF spectrum fragment the band allocations in ways unknown in lower regions. Finally, these passive allocations are denser in the 100-GHz region because molecular resonances that are of interest to astronomers and environmental scientists are more densely concentrated above 100 GHz than below [22].

WRC-2000 and succeeding conferences have defined 18 bands with coprimary passive allocations above 100 GHz. In some, passive allocations are coprimary with terrestrial fixed and mobile services and, in some others, only with other services, including intersatellite links. These coprimary bands cover 58% of the spectrum in this region. As a result, 77% of the spectrum in 100–275 GHz has either primary of coprimary passive allocations.

The ITU regulations define three basic types of passive services with such allocations that broadly classify the spectrum stakeholders described in Section II: RAS, EESS, and Space-Exploration Service (SES). The RAS is the oldest and involves Earth-based sensors looking at radio sources from sources far away from the Earth. In practice

Table 2 Prohibited Bands According to RR5.340 in Different Spectrum Regions

Band	Frequency (GHz)	Number of RR5.340 Passive Blocks	Fraction of Band Passive
UHF	0.3–3	2	1%
SHF	3–30	3	2%
EHF	30–300	15	15%

[5]Primary users are the only entities that can legitimately use a portion of the spectrum and are entitled to protection from harmful RFI from secondary users. In case of multiple coprimary allocations, the coprimary users need to coordinate with each other to avoid harmful RFI.

Table 3 Bands Above 100 GHz With Mobile or Fixed Allocations With Radio Astronomy Service (RAS) Coprimary Passive Allocations

Band (GHz)	102-109.5	111.8-114.5	141-148.5.8	151-155.5	155.5-158.5	209-226	252-265
Bandwidth (GHz)	7.5	2.45	7.5	4.5	3.5	3	13
Active co-primary allocation				Fixed/Mobile			
Passive co-primary allocation	RAS	RAS	RAS	RAS	RAS, EESS	RAS	RAS

at frequencies above 100 GHz, atmospheric absorption of such signals is a major issue, so the best locations are high-altitude arid sites. In particular, Chile's Atacama Desert is a major location for such observatories. There are few observatories in the spectrum in U.S. territory, and the only one near a U.S. urbanized area is the Arizona Radio Observatory at Kitt Peak about 80 km from Tucson, AZ, USA. Traditionally, RAS observatories have been protected from active users of the same bands by coordinating the siting and parameters of the transmitter within an established "coordination zone" [59]. National spectrum regulators establish zones around radio telescopes in which all transmitters need prior discussion with the radio telescope operators before they can be installed. The size of these coordination zones depends on both the frequencies being used at the radio telescope and the specific terrain around it. Indeed, RAS antennas point upward and, thus, can only receive power from terrestrial transmitters that are in or near a line of sight from the antenna; therefore, assessing transmitter locations, direction, and power levels in coordination areas is of utmost importance. Table 3 summarizes the allocations with RAS as the coprimary user for fixed/mobile users, which already potentially represent a first option for spectrum sharing with terrestrial active users. Finally, an emerging source of possible RFI for RAS antennas is represented by aerial vehicles, e.g., airplanes or unmanned aerial vehicles (UAVs), which maintain connectivity with the ground.

Differently from RAS systems, EESS antennas are on nongeostationary satellites at orbit heights of 400–800 km and point toward a large area on the Earth, although some limb sensing antennas point toward the horizon. EESS satellites make observations throughout their orbits, thus, could be affected by sidelobe or scattered power from terrestrial radio systems in their bands, and, thus, are the most difficult class of passive systems to protect, both from regulation and technological standpoints.

The unusual density of passive bands above 100 GHz fragments the available spectrum, forbidding or complicating the use of large contiguous bandwidths. These conditions currently hold in the 100–275-GHz band, as shown in Fig. 1.

1) The largest bandwidth with a present fixed or mobile allocation but no coprimary passive allocation is 8.2 GHz (191.8–200 GHz).
2) The largest contiguous bandwidth possible for active use (but not necessarily fixed or mobile allocations) without overlapping an RR5.340 band is 32.5 GHz (116–148.5 GHz).
3) The largest bandwidth for active use without overlapping any band with a EESS allocation is 26.25 GHz (122.25–148.5 GHz).

Thus, the use of bandwidth greater than 26.25 GHz for active use will require sharing with a primary or coprimary passive service, motivating the development of technological solutions for active/passive spectrum sharing. To extend active uses to 32.5 GHz, active and passive users will need to share RR5.340 bands. Doing so will not only require technological innovations but also the development of new policies. An apt starting point for such policies would be research findings that indicate bands less likely to be subjected to interference and be ratified by ITU-R. The process involves placing the issue on an agenda at a WRC conference, followed by discussion and (in case) approval at the next WRC conference. It is worth noting that WRC conferences happen every four years, which reduces the speed of the overall process.

C. ITU-R Resolution 731 and Spectrum Sharing Policy

At WRC-2000, the U.S. and CEPT proposals also included a provision to study whether sharing of the allocated passive bands with active services was possible without harmful interference. In 2000, on the eve of the commercial introduction of 3G/Universal Mobile Telecommunications System (UMTS) cellular technology, such studies were complicated by the fact that there were few indications of what meaningful telecommunications applications above 100 GHz, or even what data rates would be required in the long term for either mobile links or the backhaul. Resolution 731 [26] was approved as a compromise between the suggested language of the U.S. and CEPT on spectrum sharing. It states that ITU-R should study possible sharing of the passive bands above 71 GHz with other spectrum uses, and such sharing must not expose the passive service to interference levels greater than those specified by ITU-R recommendations [23], [24], [25]. At WRC-19, Resolution 731 was then updated to add new provisions for above 275 GHz, but its provisions within the 71–275-GHz spectrum remained the same, except for updating references to other ITU-R documents.

Resolution 731 specifies explicit interference criteria for EESS [23] and RAS [24], [25]. In the case of EESS, the criteria given are a triplet of numbers for each protected band which specifies: 1) the reference bandwidth over which interference power should be measured; 2) the maximum permitted interference level; and 3) the percentage of the Earth's surface area or time in which the permissible

interference level may be exceeded. These power levels are defined at the terminals of the receiving antenna in the satellite. They represent the total power received from the area of the Earth that is viewed by the antenna's footprint, including its sidelobes. A separate ITU-R document [60] gives typical satellite parameters, such as orbit height and antenna characteristics, but does not presently cover every possible band (although an update is in progress [61]). The analysis of the available literature on EESS, however, does not exhaustively clarify if all passive satellites have interference vulnerability comparable to that specified in this document. It is also not clear whether there is public information available on all passive satellites entitled to interference protection and their parameters, including orbit parameters.

Finally, Resolution 731 also contains the following provision: "to the extent practicable, the burden of sharing among active and passive services should be equitably distributed among the services to which allocations are made" [26]. This implies that, when developing sharing strategies, both the active and passive users have an obligation to cooperate to increase the overall use of the spectrum while also achieving the user-specific objectives. Nonetheless, passive satellite systems do not have the same level of flexibility as active users. The design of satellites and scientific equipment is a multiyear effort, and careful planning needs to be factored into the engineering of the RF components. Once in orbit, there is little or no possibility to change operating parameters and adjust transceiver systems to react to new or unforeseen interfering signals. As of today, most passive satellites orbiting are expensive units, with a mission lifetime spanning five to 15 years. It is also difficult to change parameters for satellites that are planned but not launched yet, even if consensus on the policy and sharing technologies is reached. So far, there has been no ITU-R discussion on the concept of "burden sharing" as introduced in Resolution 731 even though this holds long-term potential for improving spectrum sharing capability.

IV. INTERFERENCE ABOVE 100 GHz: LINK BUDGET ANALYSIS

As discussed in Section III, there exist some bands in which the active users are forbidden from emitting any RF signals. Herein, we present numerical results that highlight scenarios in which harmful interference arises, and deployments in which the same is rendered void. We first describe our modeling approach (see Section IV-A), based on ITU channel models, and then the results (see Sections IV-B and IV-C). Notably, we analyze terrestrial and aerial links as they represent typical communication and interference scenarios, e.g., with a backhaul link on the ground generating RFI toward a satellite.

A. System Model

We consider the system model shown in Fig. 5: a terrestrial link between two ground stations (e.g., a terrestrial backhaul link [16], [62]), potentially interfering with a satellite orbiting over the terrestrial deployment area. The ground stations are equipped with directional antennas and can use multiple digital modulations, bandwidths, and carrier frequencies, as shown in Table 4.

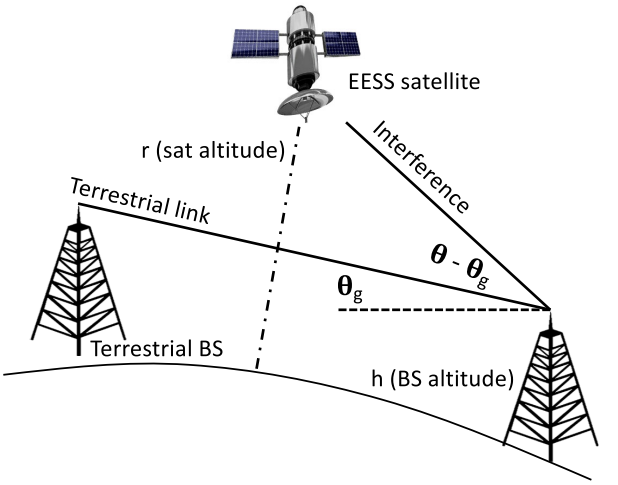

Fig. 5. *System model.*

For the terrestrial link, the received power $P_{\text{rx},g}(f,d)$ (in dB) can be expressed as a function of the distance d and the carrier frequency f

$$P_{\text{rx},g}(f,d) = P_{\text{tx},g} - L(f,d) + G_{g,\,\text{tx, max}} + G_{g,\,\text{rx, max}} \quad (4)$$

where $P_{\text{tx},g}$ is the transmit power of the ground transmitter, L is the path loss for a terrestrial link, and G is the antenna gain. We assume, without loss of generality, that the transmitter and receiver are aligned and experience the maximum antenna gain.

For the Earth–space link, the received power at the satellite, as a result of the interference from the ground station, can be expressed as (in dB)

$$P_{\text{rx},s}(f,d,\theta,\theta_g) = P_{\text{tx},g} - L(f,d) + G_{\text{tx}}(\theta-\theta_g) + G_{\text{sat}}(\theta-\theta_g) \quad (5)$$

where L is the path loss for an Earth–space link, G is the antenna gain, θ_g is the tilt of the ground

Table 4 System Parameters

Parameter	Value
Channel model	Based on ITU-R [63]–[66]
Antenna gain model	Based on ITU-R [69]
$G_{g,i,\max}, i \in \{\text{tx}, \text{rx}\}$	40 dBi
G_{sat}	$\{20, 40\}$ dBi
$P_{\text{tx,g}}$	$\{18.6, 33.4\}$ dBW (see Section IV-C)
f_c	{150, 183, 230} GHz
Noise PSD	$N_0 = -160$ dBW
Modulation	16-QAM, 64-QAM, 256-QAM, 1024-QAM
Bandwidth	Based on Fig. 4

transmitter antenna, and θ is the elevation angle between the ground transmitter and the satellite, as shown in Fig. 5.

We model the terrestrial and Earth–space path loss using ITU path loss models [63], [64], [65], [66], which include the conventional free-space path losses or spreading losses and the molecular absorption losses. These models are generally considered for the development of ITU recommendations and show consistency with other methods (e.g., based on the HITRAN database [11]) in the frequency range of interest (even though they diverge at higher frequencies) [67]. The free-space attenuation L_{spr} is due to the expansion of the wave as it propagates through the space and is calculated (in dB) as [63]

$$L_{\text{spr}}(f, d) = 92.45 + \log(fd) \tag{6}$$

where f is the frequency of the signal in GHz and d is the propagation distance in km. For Earth–space slant paths, this distance is

$$d = \sqrt{R^2 \sin^2\theta + 2Rr + r^2} - R\sin\theta \tag{7}$$

where r is the satellite altitude, θ is the elevation angle, and R is the Earth radius [68].

The molecular absorption losses are due to the interaction of the RF signal with air molecules. As mentioned in Section II-A, certain frequencies of interest result in greater resonance with specific molecules, leading to a frequency-dependent absorption loss. At frequencies above 100 GHz, the main contributor to absorption loss is water vapor [11]. Thus, the specific gaseous attenuation at height h is given by $\gamma(h) = \gamma_o(h) + \gamma_w(h)$ (dB/km), where $\gamma_o(h)$ and $\gamma_w(h)$ are the specific attenuation due to dry air and water vapor, respectively [64]. Due to the inherent frequency-selective and medium-dependent nature of absorption losses, it is dependent both on the frequency of the RF signal and the characteristics of the medium through which the signal travels (such as temperature, pressure, humidity, and density). For different Earth–space slant paths, the signal traverses different atmospheric heights, which lead to different temperatures and pressures [65]. Taking into account these factors, the total absorption loss L_{abs} is then calculated as

$$L_{\text{abs}} = \int_0^r \frac{\gamma(h)}{\sqrt{1 - \cos^2\theta(h)}} dh \tag{8}$$

where $\gamma(h)$ is the specific gaseous attenuation at height h and $\theta(h)$ is the local apparent elevation angle at height h, which depends on the refractive index at that height [66]. Combining these, the total path loss is then

$$L = L_{\text{spr}} + L_{\text{abs}}. \tag{9}$$

The antenna gain model also follows ITU recommendations. Notably, we consider the model in [69] for above 70 GHz, which models the gain as a function of the off-axis angle θ, the carrier frequency f_c, and the maximum gain $G_{\max}$ (in dB). The ITU model first computes the antenna diameter D as a function of $G_{\max}$ as

$$D \approx \lambda \cdot 10^{\frac{G_{\max} - 7.7}{20}} \tag{10}$$

where $\lambda = c/f_c$ is the wavelength. Then, it defines the first-lobe gain G_1 as

$$G_1 = 2 + 15\log_{10}\left(\frac{D}{\lambda}\right). \tag{11}$$

In the case of $D/\lambda > 100$, the gain G as a function of the angle θ is computed as

$$G(\theta) = \begin{cases} G_{\max} - 2.5 \cdot 10^{-3}\left(\frac{D}{\lambda}\theta\right)^2, & 0 \le \theta < \theta_m \\ G_1, & \theta_m \le \theta < \theta_r \\ 32 - 25\log_{10}(\theta), & \theta_r \le \theta < 120^\circ \\ -20, & 120^\circ \le \theta < 180^\circ \end{cases} \tag{12}$$

where

$$\theta_r = 15.85\left(\frac{D}{\lambda}\right)^{-0.6} \tag{13}$$

and

$$\theta_m = \frac{20D}{\lambda}\sqrt{G_{\max} - G_1}. \tag{14}$$

If $D/\lambda \le 100$, instead, the gain is

$$G(\theta) = \begin{cases} G_{\max} - 2.5 \cdot 10^{-3}\left(\frac{D}{\lambda}\theta\right)^2, & 0 \le \theta < \theta_m \\ G_1, & \theta_m \le \theta < 100\frac{\lambda}{D} \\ 52 - 10\log_{10}\left(\frac{D}{\lambda}\theta\right) & \\ \quad - 25\log_{10}(\theta), & 100\frac{\lambda}{D} \le \theta < 120^\circ \\ -10\log_{10}\left(\frac{D}{\lambda}\theta\right), & 120^\circ \le \theta < 180^\circ. \end{cases} \tag{15}$$

The signal-to-noise ratio (SNR) $\Gamma = P_{\text{rx},i}/(N_0 B)$, $i \in \{g, s\}$ is computed using a noise power spectral density (PSD) $N_0 = -160$ dBW. Here, we consider a noise model based on empirical measurements on the receivers in the TeraNova platform [70], where the electronic noise temperature of the system dominates the noise temperature

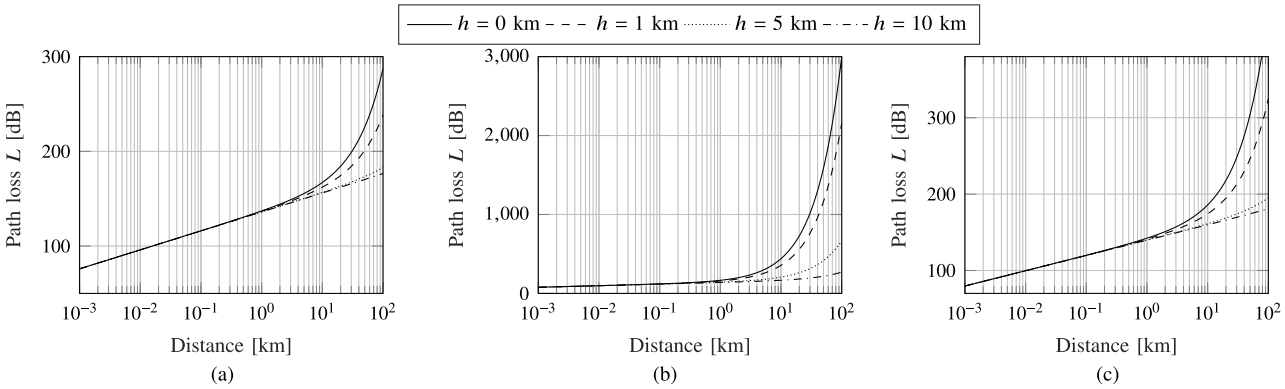

Fig. 6. *Path loss L as a function of traveled distance for terrestrial links and different altitudes h. (a) f_c = 150 GHz. (b) f_c = 183 GHz. (c) f_c = 230 GHz.*

due to molecular absorption, and the overall amplitude noise follows a Gaussian distribution. For B, we consider the bandwidth that is required to achieve a 1-Tb/s data rate with a certain modulation and coding scheme, as shown in Fig. 4(a) and (b) (see Section II). We then utilize the SNR to estimate the error rate probability for specific digital modulation and coding rates [71].

B. Path Loss Analysis

We first analyze the path loss for the terrestrial and Earth–space links.

1) Terrestrial Links: Fig. 6 shows the path loss at three different carrier frequencies for a link between two ground stations at different altitudes. The path loss curves have a typical L-shaped trend, as the spreading loss increases logarithmically with the distance (thus linearly with respect to the logarithmic plots in Fig. 6), while the absorption loss is linear with the distance (thus exponential in the plots of Fig. 6). This can be seen also by comparing the path loss at different altitudes. At higher altitudes, the atmosphere is less dense; the absorption loss reduces accordingly. As shown in Fig. 6, the path loss for $h = 10$ km maintains a logarithmic trend with the distance, while the L-shape is more evident for the path loss at $h = 0$ km. Finally, the path loss is similar for $f_c = 150$ GHz and $f_c = 230$ GHz, with the latter having a slightly higher spreading loss. Instead, when considering $f_c = 183$ GHz [see Fig. 6(b)], the impact of the absorption is dominant, as this frequency corresponds with a water vapor absorption peak. The path loss due to absorption is again reduced at higher altitudes due to a less dense atmosphere.

To further investigate the interplay between spreading and absorption loss, Fig. 7 reports the distances (in km) at which the absorption loss L_{abs} becomes larger than the spreading loss L_{spr}, for different frequencies and altitudes of the link. These results indicate that—outside absorption peaks—the contribution of L_{abs} is smaller than that of L_{spr} even for tens of km, even for the dense atmosphere at $h = 0$ km, demystifying the claim that communications in the above 100-GHz band are limited by the absorption phenomena.

2) Earth–Space Slant Paths: The different compositions and densities of the Earth's atmosphere at different altitudes have an impact on the path loss trend for Earth–space paths. Fig. 8 reports the path loss L for three different frequencies, as a function of the satellite altitude and the elevation angle between the ground station and the satellite.

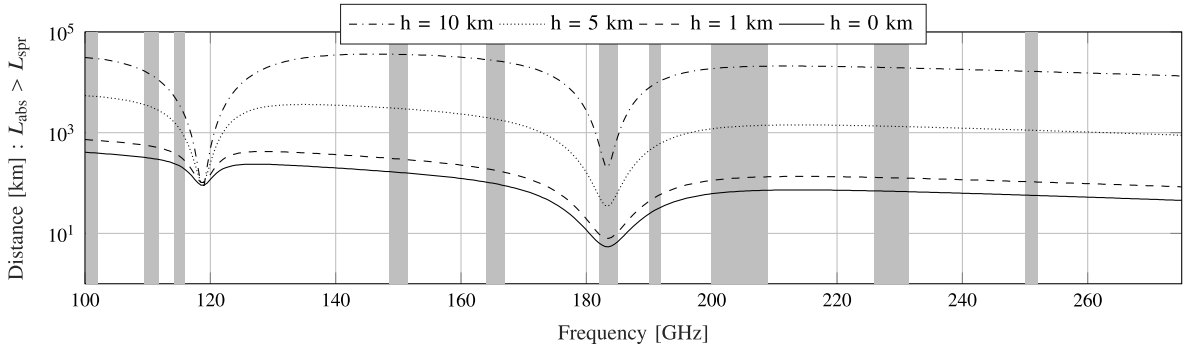

Fig. 7. *Distance at which $L_{abs} > L_{spr}$. The dark region corresponds to RR5.340 bands.*

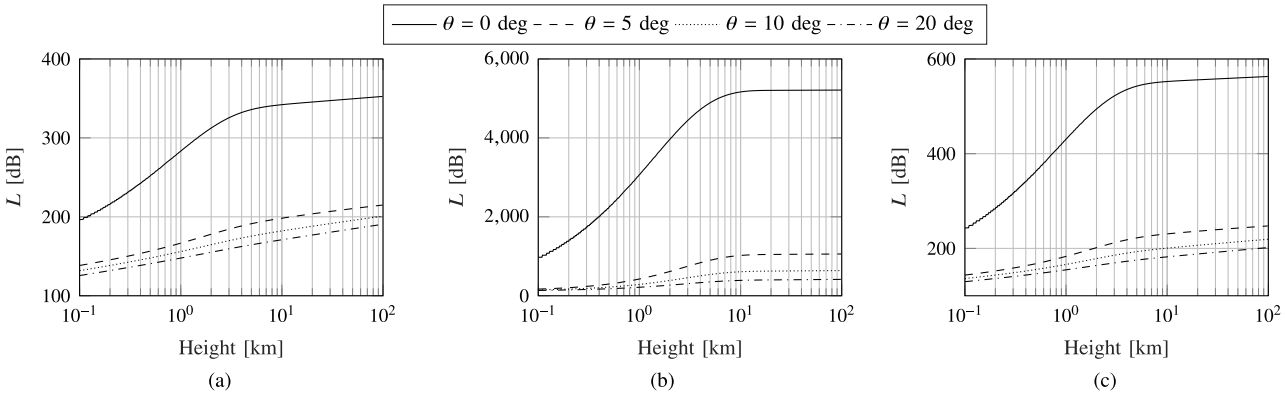

Fig. 8. *Earth–space path loss as a function of the satellite height for different elevation angles θ. (a) f_c = 150 GHz. (b) f_c = 183 GHz. (c) f_c = 230 GHz.*

The curves exhibit a reverse L-shaped trend, especially for an elevation of 0°. This shows that there exist two regimes for path loss. Below a certain altitude threshold, which is at most 10 km for the elevation of 9° and $f_c = 183$ GHz, the path loss is affected by the combined spreading and absorption losses. This leads to a much higher path loss for $f_c = 183$ GHz [see Fig. 8(b)] than $f_c = 150$ and 230 GHz. Above this threshold, however, the less dense atmosphere leads to a reduced impact of the absorption loss L_{abs}, with the dominant contribution given by the spreading loss L_{spr}. This behavior is more evident for configurations with the satellite at a lower elevation, as the signal has to travel through a thicker portion of the Earth's atmosphere. The higher path loss for lower elevation angles is key to reducing interference from ground stations to satellites, as we discuss in Section IV-C.

C. Link Budget and RFI Analysis

To identify a meaningful transmit power value for the ground station in the interference analysis, we analyze the link budget for a terrestrial link that supports a data rate of 1 Tb/s with a bit error rate (BER) smaller than 10^{-5}. We consider the system model described in Section IV-A, with the parameters from Table 4, and the bandwidth for different modulations shown in Fig. 4(b).

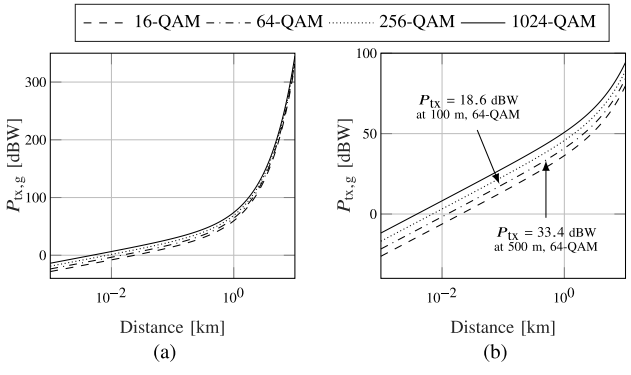

Fig. 9. *Transmit power $P_{tx,g}$ to achieve a 1-Tb/s data rate with a bit error rate smaller than 10^{-5} for different modulations and as a function of the distance between the terrestrial transmitter and receiver. (a) f_c = 183 GHz. (b) f_c = 230 GHz.*

Fig. 9 reports the transmit power $P_{\text{tx},g}$ that satisfies the required constraints for $f_c = 183$ GHz and $f_c = 230$ GHz, and four different QAM modulation orders. Considering that the number of MIMO streams supported by the link depends on the diversity of the physical channel and not on the wireless link design itself, we compute the target $P_{\text{tx},g}$ by considering the average of the transmit power required with two, four, or eight MIMO channels.

As expected, the impact of the higher absorption loss at 183 GHz translates into a higher required $P_{\text{tx},g}$ than at 230 GHz, in particular for transmitter–receiver distances larger than 1 km. In addition, high-order modulations need a higher $P_{\text{tx},g}$ than low-order modulations, with an average 14.46-dB gap between 16-QAM and 1024-QAM. This disparity exists in spite of the reduced bandwidth requirements with high-order modulations to achieve the target rate of 1 Tb/s.

In the following, without loss of generality, we consider two arbitrary reference values for $P_{\text{tx},g}$, i.e., $P_{\text{tx},g} = 18.6$ dBW, which enables a date rate of 1 Tb/s with 64-QAM at 100 m, and $P_{\text{tx},g} = 33.4$ dBW, which corresponds to 1-Tb/s data rate at 500 m, again with 64-QAM. These distances are typical representations of a backhaul link in a dense, urban environment. While we acknowledge that such transmit power levels (i.e., 72 W and 2.18 kW) are not feasible at the moment in above-100-GHz devices, they allow us to speculate on interference levels that orbiting satellites may experience in a typical 6G deployment. Similar values are reported for transmit power and effective isotropic radiated power in current sub-6 GHz and lower mmWave backhaul deployments [72], [73].

Table 5 lists the satellite that, for a given frequency band, occupies the lowest altitude orbit. The maximum permissible interference level is defined in [23]. The RFI level changes according to whether the scan is performed

Table 5 Passive Sensing Satellites in Different Bands Above 100 GHz With the Maximum Interference Level Set in [23]. *N* Stands for Nadir Scan, *C* for Conic, and L for Limb

Band [GHz]	Maximum Interference Level [dBW]	Lowest Satellite Altitude [km]
115.25-122.25	−166 (N), −189 (L)	705 Aura (NASA) [74]
148.5-151.5	−159 (N), −189 (L)	705 Aqua (NASA) [75]
155.5-158.5	−163 (N,C)	817 MetOp (EUMETSAT) [76]
164-167	−163 (N,C), −189 (L)	407 GPM Core Observatory (NASA/JAXA) [33]
174.8–191.8	−163 (N,C), −189 (L)	407 GPM Core Observatory (NASA/JAXA) [33]
226-231.5	−160 (N,C), −194 (L)	705 Aura (NASA) [74]
235-238	−194 (L)	705 Aura (NASA) [74]

in the nadir, conic, or limb mode, i.e., according to the orientation and angle between the ground RFI emitter and the antenna of the satellite under consideration. With a nadir scan, the satellite sensor and/or antenna points to the ground directly below the satellite (i.e., the nadir direction). With a limb scan, the sensor and/or antenna points to the edge of the Earth as seen by the satellite. With a conic scan, the satellite can sense in different directions (cones or beams) over time. The RFI threshold is also defined independently on the specific scientific mission and the altitude at which satellites orbit. Therefore, we consider this as a reference for harmful RFI in the next paragraphs.

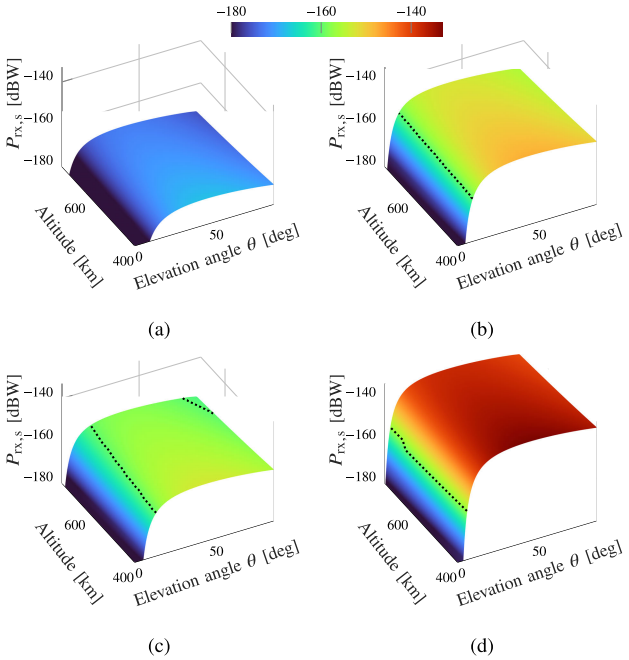

Fig. 10. ***RFI power $P_{rx,s}$ at a satellite, as a function of satellite altitude and elevation angle with respect to the ground station, for different values of $P_{tx,g}$ and G_{sat}. The dotted line represents the combinations of altitude and elevation angle values that lead to $P_{rx,s} > -160$ dBW (see Table 5). $f_c = 230$ GHz, and $\theta_g = 0°$. (a) $P_{tx,g} = 18.6$ dBW and $G_{sat} = 20$ dBi. (b) $P_{tx,g} = 18.6$ dBW and $G_{sat} = 40$ dBi. (c) $P_{tx,g} = 33.4$ dBW and $G_{sat} = 20$ dBi. (d) $P_{tx,g} = 33.4$ dBW and $G_{sat} = 40$ dBi.***

Fig. 10 analyzes the RFI for satellites performing a scan at $f_c = 230$ GHz. We assume nadir/conic operations, for which the corresponding RFI threshold is -160 dBW. Herein, the ground station antenna has a tilt $\theta_g = 0°$. In addition, the satellite altitude r ranges from 407 to 720 km, and we consider the two power levels identified in Fig. 9(b), two different (and constant) gain G_{sat} values for the satellite antenna (i.e., 20 and 40 dB), and an elevation angle θ between the satellite and the ground station that varies between 0° and 90°.

With the lowest transmit power and satellite antenna gain (i.e., 18.6 dBW and 20 dBi, respectively), the interference never exceeds the harmful RFI threshold, as shown in Fig. 10(a). However, when the gain of the satellite antenna increases to 40 dBi, as shown in Fig. 10(b) and (d), the interference threshold is exceeded when the satellite orbits above a certain threshold elevation angle, θ_{th} (represented by the dotted line). The value of θ_{th} increases with the satellite altitude. For $P_{\text{tx},g} = 18.6$ dBW [see Fig. 10(b)], it ranges from 9.73° at 400 km to 12.26° at 720 km. For $P_{\text{tx},g} = 33.4$ dBW [see Fig. 10(d)], it varies from 6° for 400 km to 6.64° for 720 km.

Finally, for $P_{\text{tx},g} = 33.4$ dBW and $G_{\text{sat}} = 20$ dBi [see Fig. 10(c)], satellites at lower altitudes (i.e., below 645 km) experience harmful RFI above the ITU-defined threshold for angles above 13.89° (for 400 km) and 19.3° (for 645 km). The trend is different for higher altitude satellites, for which there also exists a region at high elevation angles in which the interference is below −160 dBW. Namely, satellites orbiting above 645 km experience RFI above threshold in for elevation angles θ between 19.3° and 89° (for $r = 645$ km) and between 21.74° and 81.54° (for $r = 720$ km).

To better understand the elevation-dependent RFI trend, we present, in Fig. 11, the ground station antenna gain G_g (dotted, left axis), the path gain $-L$ (dashed, right axis), and the overall received RFI $P_{\text{rx},s}$ for $f_c = 230$ GHz, $P_{\text{tx},g} = 33.4$ dBW, $G_{\text{sat}} = 20$ dBi, and $r = 700$ km. It is worth

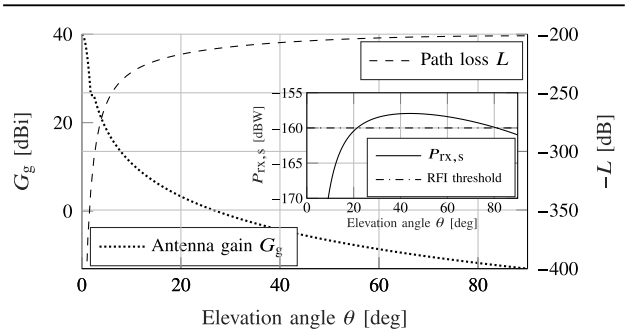

Fig. 11. ***Antenna gain G_g, path gain $-L$, and received power $P_{rx,s}$ for different elevation angles, satellite height $r = 700$ km, $f_c = 230$ GHz, $G_{sat} = 20$ dBi, and $P_{tx,g} = 33.4$ dBW.***

noting that, for the same satellite altitude r, the distance between the satellite and a particular ground station is greater for lower elevation angles, i.e., when the satellite is closer to the horizon. In addition, the signal has to travel through a thicker portion of the Earth's atmosphere, further increasing the contribution of the absorption loss. Therefore, even if the antenna gain of the ground station antenna is maximum at $\theta = \theta_g = 0°$, the high path loss leads to an RFI below the defined threshold. The path loss, however, decreases faster than the gain as a function of the elevation angle θ, as shown in Fig. 11. This leads to an increase in $P_{\text{rx},s}$, which—in this specific case—exceeds the ITU threshold for $\theta > 21°$. Finally, the path loss flattens for elevation angles above 50°, while the antenna gain decreases logarithmically with θ. Therefore, there can be combinations of path loss, transmit power, and antenna gain values that lead to RFI being below the ITU threshold for high elevation angles (i.e., for the satellite orbiting above the ground station).

We also consider the case in which the ground station antenna points toward the sky with a positive tilt θ_g. This is a typical representative of 6G nonterrestrial use cases, such as satellite-assisted cellular networks [77], the space Internet [78], and drones and UAV aerial networks [79], [80]. Fig. 12 reports the received power at the satellite for $P_{\text{tx},g} = 18.6$ dBW and $G_{\text{sat}} = 20$ dBi, and the antenna on the ground tilted by $\theta_g = 30°$ and $\theta_g = 60°$. Notice that, with $\theta_g = 0$, the RFI for this configuration of transmit power and satellite gain does not exceed −160 dBW [see Fig. 10(a)]. Our analysis shows that there exists a tilt angle $\theta_{g,\text{th}} = 7.2$ for which combinations of $\theta_g \geq \theta_{g,\text{th}}$, θ, and r lead to RFI above the threshold. In particular, the satellite receives RFI as high as −127 dBW for $\theta_g = 30°$ [see Fig. 12(a)] and −119 dBW for $\theta_g = 60°$ [see Fig. 12(b)].

These analyses indicate that directional antennas can come with mixed blessings: while the combination of directivity and high atmospheric absorption helps to reduce RFI in some scenarios (low satellite elevation), the same can lead to extremely high RFI for higher satellite elevation and nonterrestrial communications scenarios. Finally, while we consider ground-to-satellite RFI herein, similar insights can be derived when investigating interference from aerial sources toward ground passive scientific infrastructure, e.g., for radio astronomy. Indeed, while terrestrial radio astronomy sites are generally isolated and in remote locations, sidelobes (or, more rarely, main lobes) from aerial sources have the potential to generate harmful interference to passive terrestrial stations, as discussed in Section III.[6]

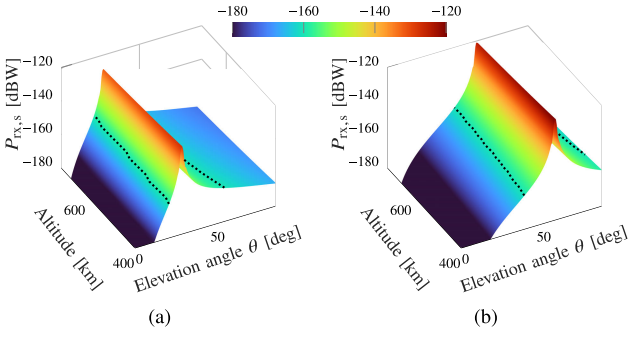

Fig. 12. *RFI power $P_{rx,s}$ at a satellite, as a function of satellite altitude and elevation angle with respect to the ground station, for different values of the ground antenna tilt. The dotted line represents the combinations of altitude and elevation angle values that lead to $P_{rx,s} > -160$ dBW (see Table 5). $f_c = 230$ GHz, $P_{tx,g} = 18.6$ dBW, and $G_{sat} = 20$ dBW. (a) $\theta_g = 30°$. (b) $\theta_g = 60°$.*

V. SPECTRUM SHARING TECHNIQUES ABOVE 100 GHz—CHALLENGES AND OPPORTUNITIES

The results of Section IV highlight that there exist scenarios in which active transmissions can create interference toward passive users, despite the directional nature of the signals and the high absorption and spread loss. At the same time, however, they suggest that in-band sharing in the spectrum above 100 GHz may be possible, thanks to the combination of the molecular and spreading path losses and the directional transmissions. Therefore, to enable dynamic spectrum sharing solutions, it becomes necessary to identify some technological enablers that allow network operations in a regime where: 1) interference is reduced or eliminated or 2) shared usage is enabled on a spatial, time, or frequency/band basis. The next paragraphs discuss the technological challenges to spectrum sharing above 100 GHz, with prospective solutions that span from devices and RF circuits engineering (antenna solutions and innovative intelligent surfaces) to the design of communication and sensing stacks. Note that some of these technologies are used—or can be used—also in other frequency bands, but they often require adaptations or addressing specific engineering challenges to be effective or feasible above 100 GHz, as we discuss in the Research Challenges paragraphs of this section.

A. Challenges to Spectrum Sharing Solutions Between Active and Passive Users Above 100 GHz

Spectrum sharing has been widely studied in the sub-6-GHz domain, as mentioned in Section I [10], [84], [85], [86]. A significant effort has been put into identifying spectrum sharing solutions, for example, in the context of radio access network (RAN) sharing among multiple 5G operators [84]. So far, however, most of the research has focused on sharing among active users and, in particular, between communications users. As mentioned above, several of the techniques investigated for the bands below

[6]Notice that large satellite constellations also have the potential to affect ground-based *optical* telescopes used for astronomy and planetary defense, i.e., to track satellites and near-Earth asteroids. However, it has been found that the impact from low Earth orbit satellites is quite manageable, as their reflected sunlight is rarely bright enough to cause major problems, except when they are very close to the horizon where these telescopes rarely operate [81].

6 GHz and active users sharing do not necessarily apply to sharing among active and passive users above 100 GHz or require solving significant engineering challenges.

For example, one of the main areas of research is cognitive radios [85]. In this approach, dynamic spectrum access of secondary users over resources primarily destined for other users is enabled with a two-step approach. The first step involves sensing or collecting information on spectrum usage, thereby identifying unused portions of the spectrum and/or patterns of usage of the primary users. The second step involves secondary-user transmission. This can happen on unused resources (interweave mode) or the resources already occupied by the primary (overlay mode), possibly with some coordination to satisfy predefined interference constraints. Notably, cognitive radios have been popular in the context of improving the usage of TV white space [87]. However, the paradigm of cognitive radio cannot be applied directly to active–passive sharing above 100 GHz. The "sensing" step is challenged by several conditions. The spectrum access by passive users cannot be sensed. The increased directivity and large-bandwidth requirements of active-user transmissions make detection more complex. Along these lines, the scale (in the number of devices) envisioned for certain above-100-GHz applications [16][7] further complicates cognitive radio systems, as the overhead for coordination increases and the amount of unused resources for interweave operations decreases. Furthermore, concurrent cognitive transmissions (e.g., as overlay) may not be tolerated by some passive sensing users if further precautions are not applied to avoid exceeding harmful RFI thresholds, as discussed in Section IV.

Other techniques that are broadly considered enablers of spectrum sharing at lower frequencies and for active users cannot be directly applied in the context of active–passive sharing above 100 GHz. Nonorthogonal multiple access (NOMA) [89], which enables code- or power-based sharing of the same time and frequency resources among multiple users and has been designed for the coexistence of multiple active users. Similarly, sharing across licensed and unlicensed bands does not apply when passive users are at stake [90]. While Ramadan et al. [91] and Cho et al. [92] consider coexistence between communication users and passive RAS and EESS services, these are for frequency bands below 100 GHz.

An additional challenge is represented by the heterogeneity between the different technologies at these frequencies [10], which require either custom solutions or coordination among different standardization or technology development forums. Such coordination, however, has been shown to be previously feasible in the sub-6-GHz context, with the notable example of the CBRS band. This portion of the spectrum, which was exclusively allocated to military use (e.g., U.S. Navy radars and satellite links), is now operated according to a shared usage pattern, facilitated by an intertechnology database that keeps track of spectrum usage and grants access with high granularity.

Overall, it is clear that there exists a need to carefully design and rethink enabling technologies and strategies to allow sharing between active and passive users in the 100-GHz bands. In addition to accounting for the presence of passive users, spectrum sharing above 100 GHz should also factor in and exploit the unique characteristics of the propagation of RF signals in these bands [93]. To this end, in the next paragraphs, we discuss and review techniques that can be applied for effective and safe active/passive sharing at frequencies above 100 GHz.

B. Solutions Enabled by (Sub)Terahertz Devices and Wave Propagation

To effectively communicate at frequencies above 100 GHz, highly efficient, directional antennas are required. In such a setup, unwanted interference toward sensitive devices outside the main coverage region manifests as leaking power in the form of sidelobes. In directional antennas and uniform amplitude antenna arrays, the more directional the mainlobe, the greater the dominant sidelobe levels (SLL), or the effective power contained within the dominant sidelobes [82]. Such a manifestation of the sidelobes can be seen for a typical high-density MIMO array (8×8) in Fig. 13(a). It is seen that, while the mainlobe can be extremely directional, the major sidelobe strength can be as much as -13 dB in comparison. Thus, it is necessary to consider the entire radiation pattern of the array/antenna and develop working objectives to truncate such SLL, which contributes to interference concerns.

1) Inverse Pyramidal Arrays: Above 100 GHz, highly directive radiation and significant power output are expected for base stations (BSs) supporting massive MIMO. Thus, the main objective of device design can be tailored toward significant control over the SLL in these BSs. An intuitive method of mitigating interference in unwanted directions is to have a physical configuration within which

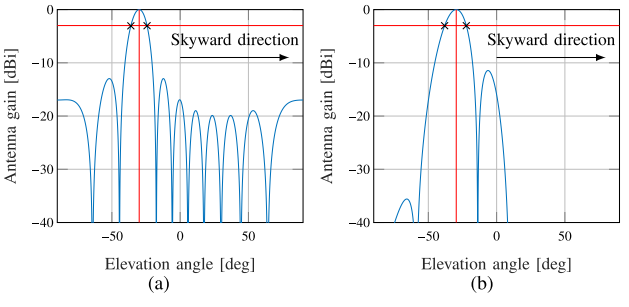

Fig. 13. ***Utilization of active suppression on the skyward directions during the array synthesis can suppress unwanted emissions. In both cases, the desired angle of steering is 30° below the horizon. (a) Conventional beamforming. (b) Smart beamforming.***

[7]Projections from the literature and market analysis point to an increase from 10^6 to 10^7 devices per km^2 when transitioning from 5G to 6G [88].

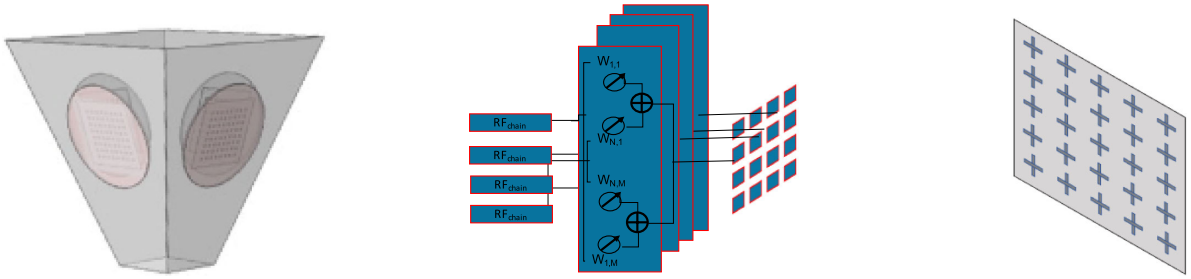

Fig. 14. *Device configurations to minimize undesired RFI. (a) Inverse pyramid design for a terrestrial BS can minimize interference with other users of interest above the BS height. (b) Hybrid or fully digital array architectures can be utilized to implement nonuniform amplitude arrays for reduced sidelobe strength [82]. (c) FSS can be incorporated to act as a passive aid to block frequencies of interest from extremely sensitive directions, for example, through a dome structure, as discussed in [83].*

the unwanted directions are generally excluded from the radiation pattern. The inverse pyramidal array design, an example of which is presented in Fig. 14(a), acts as a direct complement to the pyramidal array design [94]. In such a setup, the geometrical configuration of the array favors scan angles below the horizon, thereby minimizing the power leakage above the BS itself. A four-sided pyramidal array, similar to that in Fig. 14(a), is known to provide maximum coverage efficiency, thereby reducing deployment resources [94]. Each side of the pyramid comprises an antenna array that serves a particular sector for full coverage.

Research Challenges: It is important to note that this design can be used only in deployments with BSs altitude higher than that of the connected users. In addition, there are multiple research challenges related to building dynamic beamforming antenna arrays above 100 GHz, as we describe together with the next point.

2) Active SLL Suppression: As mentioned in Section IV, 6G BSs may be required to provide coverage in aerial scenarios. Here, the BS needs to serve users not just at lower or at equivalent altitudes to itself (e.g., other BSs and user equipments (UEs)) but also to users above in altitude, for example, UAVs. Thus, in the full 3-D coverage space, it becomes necessary to consider more active SLL suppression techniques. In conventional arrays, zero-forcing beamforming is considered a convenient technique, with which different receivers can experience orthogonal channels. In this case, the goal of the beamforming algorithm is to ensure that no signal is received in a target direction, at the cost of less control on the beam shape everywhere else. However, with fully digital or even hybrid beamforming architectures as found in current massive MIMO 5G devices [95], more robust beamforming techniques can be implemented. We present an example of a hybrid beamforming architecture that could be exploited to control interference in Fig. 14(b), with the corresponding potential far-field radiation response shown in Fig. 13(b). With knowledge of critical interference directions (where sensitive devices may be located), the array response can be tailored through interference suppression algorithms as in [96], to ensure complete suppression of leakage in critical directions, while still providing coverage to users that require service in other angular regions. As shown in Fig. 13(b), the mainlobe can be preserved, while the more problematic sidelobes can be truncated greatly.

In addition to novel array architectures, another breakthrough that is extremely important in the above 100-GHz range is the rise of intelligent reflecting surfaces (IRSs) [97]. Although the fundamental principles of IRSs are valid across the spectrum, these are increasingly relevant for the (sub-)THz band, as the greatly simplified design helps to reduce the constraints on increasing the size of the array and in its deployment [98]. For example, the reflectarray-based IRS demonstrated in [98] is composed of nearly 10 000 elements, while active RF chain-based arrays are yet below the 256-element mark [99]. By moving the burden of beamforming "off-chip" and removing the need for any RF chains, the same IRS can be shared among multiple users, as discussed in [100]. IRSs can also be manipulated to create custom beam shapes [100], and if their design is realized through a metasurface-based, subwavelength-sized meta-atoms, the level of control is increased drastically [97], [101]. Such IRSs can be utilized to create anomalous reflection [102], in which almost negligible sidelobes are produced, greatly reducing interference due to sidelobe energy and introducing new opportunities for spectrum sharing. They can also be used to redirect beams toward different directions from where originally intended, as discussed in [103].

Research Challenges: The majority of algorithms for beam design and active SLL suppression have been proposed for lower frequency systems and, thus, do not capture challenges associated with working above 100 GHz. As we move to higher frequencies, the wavelength becomes shorter, and thus, the antenna array elements become smaller; they can be more densely packed without suffering mutual coupling [50]. However, the size of every other component in the RF chain (i.e., frequency multipliers, mixers, filters, and amplifiers) does not necessarily scale by the same factor. This leads to

challenges in the packaging of such arrays above 100 GHz. Consequently, there is a need to develop new antenna array architectures. First, one could consider adopting a fully analog antenna architecture, in which one only RF chain is utilized to drive multiple antennas each with analog phase and/or amplitude control [104]. Even in that case, there are several challenges. First, broadband phase controllers that can work across large contiguous bandwidths (e.g., tens of GHz) are still being developed. Strictly speaking, some of the benefits shown in Fig. 13(b) could be achieved only with the additional manipulation of the amplitude at each antenna element [82], [105]. However, the integration of an amplitude controller (ultimately, a power amplifier) per antenna element is many times not possible again not only due to packaging but also thermal issues [99]. As a solution, innovative true-time delay controllers could be utilized, for example, by leveraging new materials, such as graphene specifically proposed for the terahertz band [106] and, accordingly, the algorithms adapted.

Many of the challenges associated with building such antenna arrays and IRSs originate in the fact that the designs demonstrated to date leverage the so-called electronic approach to sub-THz and THz devices [27], in which the limits of traditional electronic systems are pushed to operate at higher frequencies. Alternatively, again, new materials could be adopted to build arrays that leverage the properties of surface plasmon polariton waves and intrinsically operate at THz frequencies [50]. As of today, graphene-based plasmonic signal sources [107], [108], plasmonic phase, amplitude and frequency modulators [109], [110], and antennas [111] have been demonstrated. Their integration in very dense arrays with element spacing much smaller than the free-space wavelength enables ultramassive MIMO systems [112], with unprecedented control of the beam shapes and wavefronts [100]. Nevertheless, this technology is much less mature than electronic or even photonic solutions, making it a high-risk, high-reward approach. Even with IRSs, although it is much easier to scale up in size, designing high-performing, versatile analog phase shifters at such high frequencies is a challenging task [113]. Among other solutions, the utilization of plasmonic materials and hybrid structures presents an interesting direction for realizing these devices [114].

3) Passive Mitigation Techniques: In addition to preemptive suppression techniques at the BS, it is possible to address interference through passive devices that do not increase the complexity of the BS itself. From the discussions in Sections II-A and IV, it is evident that sensitive devices that require protection from unwanted interference will rarely occupy the entire spectrum of emission of the BS. For example, the presently prohibited 109.5–111.8-GHz portion of the spectrum can be specifically addressed by suppressing RFI within this 2.3-GHz bandwidth. In this regard, frequency-selective surfaces (FSSs) are devices that specifically address such sensitive specks of a frequency spectrum. As shown in Fig. 14(c), an FSS is a dense, metasurface-like configuration with resonant passive elements in an array, usually designed to intercept and interact with a bandwidth of interest [115], [116], [117]. These have traditionally been utilized to reduce the cross section of radars [115] and recently have been proposed to reduce unwanted SLLs and leakage in wideband antenna arrays above 100 GHz [118]. In addition, these have been proposed to reduce mutual coupling effects between antenna elements in densely packed antenna arrays [119]. Within the mmWave band, FSSs have attracted attention, inter alia, to act as planar lenses with enhanced directivity, low cost, and ease of deployment [116], [117]. With an FSS, it is possible to design both bandstop and bandpass filters that can be deployed without any additional complexity at the BS itself, avoiding the complexity of greater control and increased power consumption requirements. The effectiveness of an FSS depends on the relative orientation of the surface with the unwanted radiation. Thus, with proper alignment toward the dominant sidelobes that may interfere with sensitive devices, an FSS designed to act as a stopband at the sensitive portions of the spectrum can be deployed, through which the unwanted leakage can be suppressed significantly [115].

Research Challenges: While simpler than the devices needed for active SLL suppression, the main challenges associated with the passive solutions relate again to the hardware design. In particular, when implemented through metasurfaces, the design of the FSSs is not governed by well-defined equations and operating theory as, for example, the design of beamforming or beam-nulling algorithms. Instead, an "artisan"-based trial-and-error methodology is required to develop the meta-atom shape and arrangement [101], [120]. As an alternative, a library of meta-atoms designs and potential arrangements to achieve different functionalities needs to be built, which could benefit the wireless community at large. In addition, there are system-level challenges associated with deploying such devices, in terms of both network and frequency planning.

C. Solutions Based on RFI Mitigation for Passive Users

Complementary and independent of custom device design solutions, harmful RFI can be mitigated with signal processing techniques. RFI mitigation has been typically studied as a necessary step in passive sensing signal processing pipelines, to protect from undesired RF emissions in the band of interest, either intentional or unintentional. As discussed in Section II, the receivers used by several passive sensing applications (e.g., radio astronomy) have extremely high sensitivity and can pick up signals that would otherwise be considered below the noise floor [121]. In the context of spectrum sharing, RFI

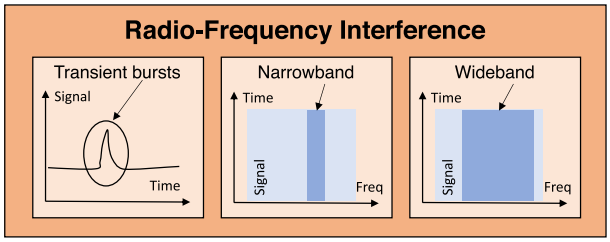

Fig. 15. ***Classification of different sources of RFI.***

mitigation puts the burden of interference management on the passive users. Therefore, while it is an essential component of the passive sensing digital signal pipeline, it represents just one of the different ingredients that need to be combined for a balanced approach to spectrum sharing. In the next paragraphs, we review general characteristics and approaches for RFI mitigation and discuss a few specific examples of RFI mitigation above 100 GHz.

RFI is generally categorized into three different classes (see Fig. 15), i.e., transient bursts, generated by impulse-like waveforms, and narrowband or wideband signals. In addition, RFI may be caused by sources that transmit in the band of interest or by out-of-band emissions. The RFI may: 1) introduce clearly identifiable distortion(s) in the gain or frequency response of the received waveform; 2) obscure the received signal, with strong and identifiable emission in the entire observed spectrum; or 3) introduce more subtle alterations in the received signals (e.g., if the RFI power is close to the noise threshold), which are harder to detect and, consequently, filtered out.

1) General RFI Mitigation Techniques: The general approaches toward RFI mitigation involve temporal, frequency, or spatial filtering or rely on specific properties of the received signals. Temporal- and frequency-domain RFIs can be detected and blocked if confined in specific time instants or subbands, for example, with threshold-based methods. For measurements of natural phenomena, whose statistical distribution is known (and often Gaussian), statistical methods can be used to identify and reject outliers that may correspond to RFI [122]. Widely used techniques include: 1) evaluating the kurtosis ratio of the received signal [123], i.e., the ratio between the fourth moment and the squared second moment (variance) of a signal, which should be equal to 3 for Gaussian signals and 2) evaluating the third and fourth Stokes parameters of the signal, which are related to its polarization and are typically small in the absence of RFI [122]. The RFI can also be detected by analyzing signals in the spatial domain. If the direction of the source of the intended signal is known, RFI can be detected through filtering signals with Angle of Arrival (AoA) outside a predefined region [121]. Importantly, as discussed above, the presence of massive-MIMO arrays in the 100-GHz region provides an ability for unprecedented angular resolution and accurate AoA detection. Alternatively, highly diffused sources without RFI exhibit a smooth behavior in the spatial and angular domains; thus, RFI can be detected and filtered by analyzing the outliers. State-of-the-art RFI mitigation systems often combine two or more of these techniques to maximize the probability of detecting RFI [124], [125], [126].

2) Use-Case-Specific RFI Mitigation Techniques: The RFI mitigation techniques need to adapt both to the characteristics of the interferer and the nature of the observation and equipment utilized. The result is that, oftentimes, general signal processing techniques for RFI mitigation need to be adapted to the specific use case [121], [126], [127], [128]. Signal processing for RFI mitigation can be run offline [129] or online [130]. While this may be a concern for the spectrum above 100 GHz, given the large bandwidth at stake, the research and development of hardware-accelerated signal processing pipelines have led to multicarrier filter banks capable of processing tens of GHz of bandwidth [131]. Similarly, mixed online and offline approaches are emerging to reap the benefits of both, e.g., for the RFI mitigation system of the next-generation Very Large Array (ngVLA) radio telescope [132]. This enables both real-time adaptability to the source and more complex signal processing offline, with applicability to very large bandwidths. While the ngVLA is expected to work in the 1.2–116-GHz band, the hardware and software techniques developed for its RFI mitigation could be reused in above-100-GHz systems as well.

Research Challenges: So far, most of the research on RFI mitigation has focused on sensing bands below 24 GHz [133], which were considered the most exposed to undesired emissions from commercial radios. This represents a potential issue for current systems operating above 100 GHz, as they are generally not equipped with RFI mitigation pipelines, which reduces the ability for sharing and coexisting with active systems. Future sensing instruments can instead be equipped with RFI mitigation mechanisms, whose design, however, is challenged by a number of elements. As previously mentioned, the large bandwidth complicates the design of real-time signal processing pipelines for RFI mitigation. In addition, the design of RF circuits is made more complex by the high-frequency and large-bandwidth requirements, which may introduce greater interference from out-of-band emissions. However, the limited multipath (or absence of it) typical of propagation above 100 GHz [134] makes spatial filtering extremely powerful, as RFI sources exhibit limited or no scattering and the number of directions to target for nulls become smaller.

D. Solutions Based on Waveform Engineering and Digital Signal Processing for Active Users

It is further possible to reduce RFI through waveform designs where the communication and sensing signals are made orthogonal to each other or are otherwise engineered to not register as interfering with each other.

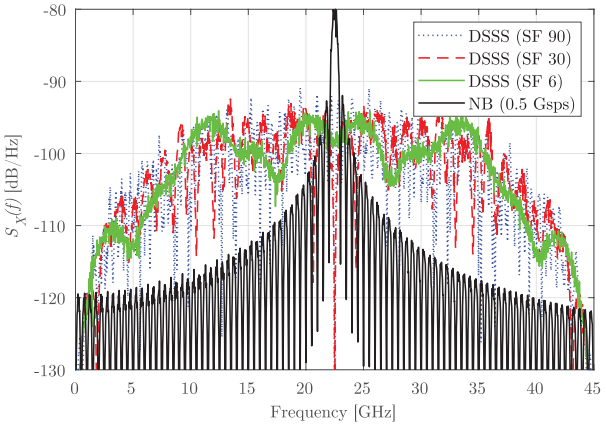

Fig. 16. ***Power spectral density of a direct sequence spread spectrum (DSSS) signal with different SFs and a narrowband signal, both modulated with 4-QAM. Figure adapted from [136].***

1) Spread Spectrum Techniques: A very large contiguous bandwidth can be leveraged to create spread spectrum waveforms, in which the communication signal can be artificially lowered to below the noise floor. Such methods have been utilized in DSSS to create efficient spectrum sharing, such as in code-division multiple access (CDMA), where a specific communication signal is multiplied by a spreading key, to artificially spread a narrowband signal over a very large bandwidth [135]. The receiver utilizes the same key to recover the signal, and all other signals within the same subspace are filtered as noise. In this setup, the larger the pseudorandom key-generating sequence, the greater the number of orthogonal signal sets that can be created. In addition, by combining multiple communication bands together, frequency hopping, similar to Bluetooth transmission, can be leveraged to create multiple windows of signal transmission that falls outside the critical bandwidth portions reserved for sensing. Ultimately, however, such spreading techniques compromise the very high data rate requirement for communication standards and would require a bandwidth, which proportionally increases with the length of the sequence, compared to that presented in Fig. 4(b).

Research Challenges: As of today, the main bottleneck in DSSS-based coexistence techniques above 100 GHz is the real-time generation of ultrabroadband spreading sequences. For example, in [136], we built and experimentally demonstrated a DSSS system for sharing between active and passive systems above 100 GHz. The framework can successfully generate sequences at 130 GHz with a 20-GHz spread bandwidth. Fig. 16 shows the PSD over frequency for a narrowband signal and DSSS signals with three different spreading factors all for a 4-QAM signal. An increase of the spreading factor leads to more uniform upper envelopes for the PSD, with peaks at about 15 dB below the peak of the narrowband signal, at the cost of achievable data rate. This effect, which is popular in tactical communications contexts to decrease the signal interception or eavesdropping probability, can also lead to received signals at the satellite sensor, which are below the RFI threshold, as further discussed in [136]. Indeed, a reduction of 15 dB in the received signal at the passive system can increase the parameter space in which active systems can coexist without exceeding the RFI threshold, e.g., compared to the configurations in Fig. 10. However, to realize this, we used a state-of-the-art arbitrary-waveform generator with data-converters operating at 92 Gigasamples-per-second at the transmitter and 160 Gigasamples-per-second at the receiver, with power requirements, size, and cost only suitable for lab testing. To overcome the bottleneck introduced by the high-speed data converters, one solution is to design fully analog DSSS chips that operate directly with analog I/Q samples in baseband or at an IF frequency. The design of such chips should be accompanied by the exploration of low-complexity real-time implementable orthogonal sequence generation algorithms.

2) Frequency-Selective Waveforms: Transmitters that can support very high peak-to-average power ratio (PAPR) can be utilized to actively remove compromised portions of the signal space from waveforms. An example where such a setup could potentially be implemented without significantly reducing the communication capacity is in OFDM [46], [47], [48]. In OFDM, groups of subcarriers are organized into resource blocks, and power allocation can be performed on a resource block level. The judicious allocation of resource blocks determines the peak capacity rate. In such a setup, it may then be possible to purposely identify subcarriers within the sensitive regions and minimize the effective power distributed to them.

Research Challenges: In alignment with many of the previous challenges, the bottleneck is posed again by the hardware and, particularly in this case, the power amplifiers. At all frequencies but particularly at frequencies above 100 GHz, power amplifiers are very sensitive to power fluctuations, and thus, carrier nulling in OFDM is many times not an option. Besides, waiting on the development of more robust amplifiers, there are other possible solutions. For example, a common waveform found in radar systems, also those at frequencies above 100 GHz, relies on continuous frequency modulation or chirp signals. Recently, our group has demonstrated the ability to utilize chirps in the chirp spread spectrum (CSS) to both transmit information even in extreme frequency-selective channels (such as those over an absorption line at THz frequencies) [137] and to build a joint communication and atmospheric radar system [138]. Differently, one could design noncontinuous frequency chirps that skip certain frequency bands to minimize the radiation in forbidden bands.

3) Orthogonal Waveforms: Another technique, only valid for the coexistence of active sensing (e.g., radar) and communication users, relies on utilizing waveforms generated in the context of orthogonal basis sets, where every signal

is independent and orthogonal to the other. One such example is the Gram–Schmidt orthogonalization [139]. In this setup, a set of M finite energy symbols is mapped to a set of N orthogonal symbols as follows:

$$s_i(t), \quad i = 1, 2, \ldots, M \mapsto \phi_i(t),\ i = 1, 2, \ldots, N;\ N \leq M. \tag{16}$$

Here, the orthogonal signals $\phi_i(t)$ are created from $s_i(t)$ through a filter bank, where the components of the previous orthonormal signals are removed from the concerned signal. Gram–Schmidt orthogonalization is actively used in most MIMO applications involving coherent detection by utilizing QR decomposition [140]. Without loss of generality, assume that the first orthogonal signal, $\phi_1(t)$, is actively selected for sensing applications. It is then possible to eliminate any interfering portions from the remaining symbols, $\{\phi_{2,}(t), \phi_N(t)\}$, used for communications. This procedure requires some level of interaction between the active sensing and communications systems to coordinate the nature of the sensing signal $\phi_1(t)$.

It is important to note that the exclusion of an orthonormal basis function does not simply remove one symbol from the possible symbol set of transmission. In fact, this makes the symbol set incomplete, reducing it from $M = 2^N$ to $M - 1 = 2^N - 1$, thus making the representation of N bits impossible. Thus, with the capability of representing only $N - 1$ bits, only $2^{(N-1)} = M/2$ symbols are required.

Here, we observe that this setup can still be utilized when required to preserve multiple sensing frequencies since there are several redundant message symbols that can be utilized and thus could be utilized without losing any further capability. Ultimately, however, the principles of utilizing the Gram–Schmidt orthonormalization require careful consideration of the richness of the basis set, the complexity of the modulation scheme, and the modifications that must be performed with regard to ensuring that the key system parameters, such as the bit error rate, the data rate, and the Euclidian separation of the constellation points, can be determined accurately and predictably.

Research Challenges: This type of solution is only applicable to future active and passive coexisting systems, as it requires coordination. As mentioned in Section III-C, this is the type of "burden sharing" expected from Resolution 731. As with the other waveform-based solutions, the computational complexity of the modulation/demodulation algorithms, the requirements of the data converters, and the potential implementation of the solution in the analog domain are aspects to be taken into account. In addition, the modulations utilized in high data rate communications often require precise inputs and constellation requirements, which makes the omission of a basis function particularly challenging. Certain parameters such as a uniform constellation, the efficiency of a message signal, and a possible noncompleteness of the symbol set could result in nonlinear distortions and reduced throughput, as discussed above.

E. MAC Layer and Networking-Based Sharing

Dynamic spectrum access can be enabled at the MAC layer and above through time and spatial sharing. In particular, it is possible to envision sharing mechanisms with different levels of integration among the technologies used by interested stakeholders of the above 100-GHz band from a fully integrated solution to a CBRS-like model.

1) Shared Active/Passive Medium Access Schemes: One option is represented by time-division multiple access (TDMA) between two or more technologies, with active and passive users sharing different time resources. For example, next-generation wireless network MAC designs may include some time slots that can be blanked for sensing [141], either active or passive. To fully exploit this flexibility, the sensing stack could be integrated into the communications stack, e.g., satellites used for commercial downlink communications could be also equipped with passive sensing systems activated on a time-sharing basis. Alternatively, passive sensing systems could be equipped with an additional sensing loop that detects when the communication link is not used and collect valid observations.

Research Challenges: It is challenging to design, deploy, and implement these approaches in practice. Indeed, they require a tight synchronization between different signal processing chains and RF circuits, which generally have a transient behavior and cannot switch on and off instantaneously [143]. Therefore, even though this is an MAC-level strategy, it requires tight coordination and innovations in the physical layer and at the device level, especially as the duration of channel access decreases with the increase of the data rate. In addition, while frequent time switching is well tolerated by packet-based communication systems [144], [145], it may not be compatible with the sensing of continuous sources of electromagnetic signals and/or long integration times. Finally, these sharing solutions are dependent on protocols that would need to be developed, tested, and standardized in the relevant forums.

2) Multiband Systems: It is also possible to design time sharing mechanisms with a granularity in the order of minutes. While these do not enable the same level of multiplexing and spectrum utilization as MAC-based strategies, they require limited or no coordination between the users of the spectrum. Notably, there are approaches in which only one of the two systems (i.e., communications or sensing) can change to adapt to the other. For example, in [142], we demonstrated the feasibility of passive/active spectrum sharing through dynamic spectrum access, with the communications stack dynamically adapting to the presence of passive sensing satellites over the deployment area. The system [as shown in Fig. 17(a)] is capable of tracking satellite mobility (e.g., the NASA Aura satellite [4]) and predict when a passive-sensing station starts

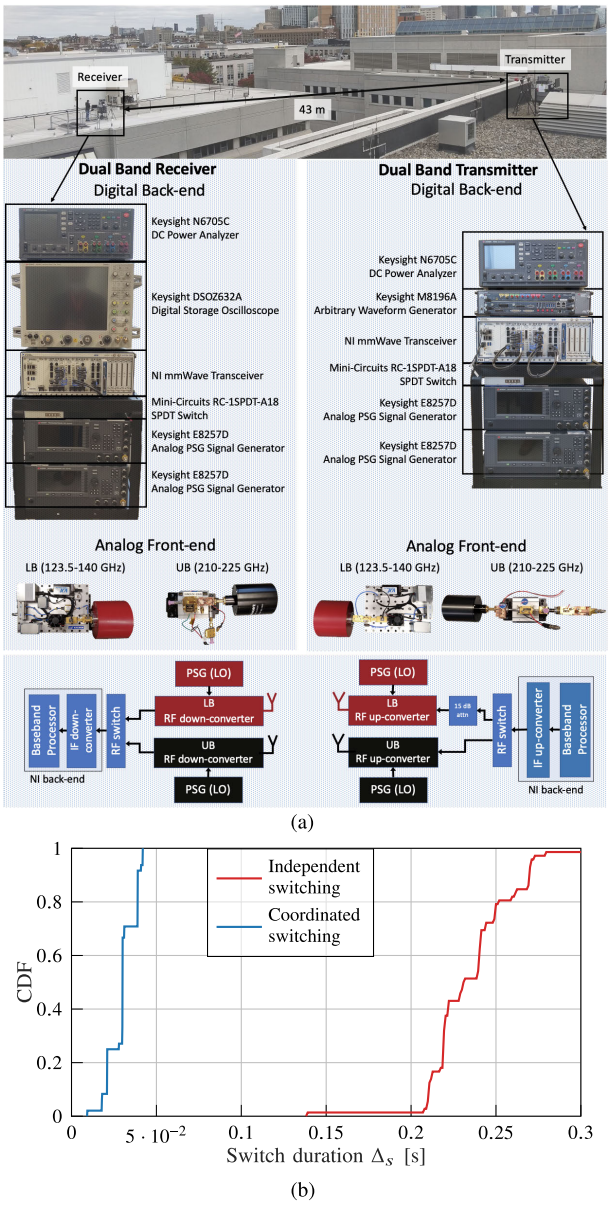

Fig. 17. ***Prototype and performance of the first dynamic spectrum access system above 100 GHz from [142]. (a) Prototype schematics of a dual-band prototype for dynamic spectrum access above 100 GHz from [142]. (b) cumulative distribution function (CDF) of the duration of a procedure to switch between bands with a centralized (coordinated) or distributed (independent) approach from [142].***

orbiting over the deployment area of the communication link. When this happens, the system switches from the band that may interfere with the satellite to another band, enabling time sharing of resources that would otherwise be unused, while introducing no harmful interference to the sensing system. This process happens with a granularity of minutes, i.e., it does not need a tight integration between the sensing and communications stacks. Nonetheless, it is important to perform the switch between bands in a timely fashion, so as to avoid downtime for the communication link. Fig. 17(b) compares the CDFs of the duration of switch events with a coordinated (or centralized) approach and an independent (or distributed) strategy. Even though this is a prototype, the system achieves low switching times (i.e., in the order of ms) with centralized switching, showing that dynamic spectrum access is feasible even in the spectrum above 100 GHz.

Research Challenges: There are several system-level challenges that need to be addressed to make these schemes scalable and practical. As for the MAC-based approaches, there is a need for protocols and standardized strategies. In this sense, the transition toward more open and programmable systems in cellular networks [146] will help embed dynamic control of the cellular stack and provide practical primitives to implement this kind of spectrum sharing. Besides this, other system-level challenges are related to security, scalability, and resource scheduling, in particular, considering the directional nature of communications above 100 GHz and the number of users that will need to be supported in 6G systems.

3) Coordination-Based Sharing: From a broader perspective, dynamic spectrum access can be generically extended to support the coexistence of multiple services, for example, through a shared, dynamic spectrum marketplace (which could be managed by the ITU or by local regulators) in which licenses can be leased dynamically, with a subsecond latency. As previously mentioned, the CBRS band proceedings have shown that coordination and preemption among different active users are feasible on a dynamic basis. Baxley and Thompson [147], [148] demonstrate a dynamic system for active/passive users sharing as part of one of the DARPA Spectrum Collaboration Challenge (SC2). The availability of fast connectivity and data bases is a key step toward the feasibility of distributed spectrum access systems that can control spectrum usage with the granularity of tens of kilohertz in bandwidth and 1 ms in time (typical values for 5G systems) [149]. Coordination-based solutions are also mentioned and evaluated in the National Research Council report on how spectrum can be used by scientific users in the 21st century [22]. The authors envision a scenario with multiple satellites for Earth exploration, each with a beam covering an area on Earth with a diameter of 30 km. The active users on the ground could coordinate with the sensing satellites through a shared database and blank the resources required for sensing on an ad hoc basis. For a constellation of 30 satellites, with the aforementioned characteristics, [22] estimates that active users can transmit in the band of interest of the passive sensing system for 99.7% of the time *without causing any interference*. Similar results are presented in [150]. This shows that spectrum sharing between active and passive users is possible, with the proper combination of policies and technologies.

Research Challenges: As for the previous higher layer techniques, most challenges arise at the system level, in particular, when considering the number of active and passive users that require coordination, the size of the

database, and the need for real-time adaptation. A promising factor is that there is a limited number of passive sensing facilities, whose position and frequency occupation are often known or predictable, and the fact that terrestrial sensing stations (e.g., for radio astronomy) are in remote locations with limited human presence. Nonetheless, any solution that has the potential to be deployed in practical scenarios needs to be tested for robustness, scalability, and security, without harming passive users in the process, while guaranteeing the data rates and quality of service levels expected for above-100-GHz communications systems. Finally, sensing- and beaconing-based coordinations (e.g., as CBRS) are challenged by the directional nature of communications above 100 GHz, which could introduce deafness to some transmissions or beacons.

VI. Conclusion

The future of technologies and policies in the spectrum above 100 GHz is being shaped by the development of new use cases and capabilities in the communications and active and passive sensing domains. In this article, we have provided the first comprehensive overview of stakeholders, policies, and technologies for spectrum sharing in a band above 100 GHz. First, we reviewed the relevance of this portion of the spectrum for sensing applications in both the active and passive sensing domains and for next-generation communication networks. We discussed the need for more bandwidth for improved performance in both sensing and communication applications, which motivates spectrum sharing approaches, and reviewed the relevant spectrum policies in this domain. We then analyzed the impact that active terrestrial users may have on passive sensing satellites, showing how spectrum sharing techniques need to protect and account for the presence of passive incumbents. Finally, we discussed possible approaches to spectrum sharing above 100 GHz, considering devices, signal processing, and higher level coordination.

Outlook—Spectrum Policies for the Next Decades: This article clearly shows that there exists a need, opportunities, and technologies to enable shared use of the spectrum above 100 GHz. In this sense, the sensing and communication communities have the opportunity to work together to evolve spectrum policies and technologies. Efforts in this direction can lead to the following.

1) Enabling experimental research on spectrum sharing between active and passive users, fully realizing the provisions in the ITU Resolution 731 [26], and jumpstarting the development of technologies for safe spectrum sharing above 100 GHz. In this sense, the development of National Radio Dynamic Zones (NRDZs) will be critical for the study of active/passive coexistence. The U.S. National Science Foundation NRDZ program seeks to establish large-scale testbeds in contexts where RF transmissions outside current regulations will not harm normal receivers. Through this program, we are developing NRDZ capabilities in Colosseum, an open-access and publicly available hardware-in-the-loop wireless network emulator [151]. Colosseum will be extended to support large-bandwidth, highly directional transmissions (such as those of interest in the spectrum above 100 GHz) and is naturally positioned for spectrum sharing studies without *any* risk of harming legitimate users of the spectrum thanks to its emulation capabilities.
2) Identifying opportunities for a sharing-aware approach for the development of future scientific sensing equipment and communication networks. For example, active engagement across different communities could lead to the establishment of sharing procedures similar to that of the CBRS band, with benefits for all parties involved.
3) Using an evidence-driven, physics-based approach to develop spectrum policies that involve sharing in the RR5.340 bands, without harming passive incumbents. ■

REFERENCES

[1] I. F. Akyildiz, J. M. Jornet, and C. Han, "Terahertz band: Next frontier for wireless communications," *Phys. Commun.*, vol. 12, pp. 16–32, Sep. 2014.

[2] P. U. Jepsen, D. G. Cooke, and M. Koch, "Terahertz spectroscopy and imaging—Modern techniques and applications," *Laser Photon. Rev.*, vol. 5, no. 1, pp. 124–166, Jan. 2011.

[3] R. Dickie, R. Cahill, V. Fusco, H. S. Gamble, and N. Mitchell, "THz frequency selective surface filters for Earth observation remote sensing instruments," *IEEE Trans. THz Sci. Technol.*, vol. 1, no. 2, pp. 450–461, Nov. 2011.

[4] J. W. Waters et al., "The earth observing system microwave limb sounder (EOS MLS) on the Aura satellite," *IEEE Trans. Geosci. Remote Sens.*, vol. 44, no. 5, pp. 1075–1092, May 2006.

[5] G. B. Taylor, C. L. Carilli, and R. A. Perley, *Synthesis Imaging in Radio Astronomy II*, vol. 180. 1999. [Online]. Available: https://www.aspbooks.org/a/volumes/table_of_contents/?book_id=292

[6] C. E. Shannon, "A mathematical theory of communication," *Bell Syst. Tech. J.*, vol. 27, no. 3, pp. 379–423, Jul. 1948.

[7] J.-S. Lee and E. Pottier, *Polarimetric Radar Imaging: From Basics to Applications*. Boca Raton, FL, USA: CRC Press, 2017.

[8] *Study on Supporting NR From 52.6 GHz to 71 GHz*, document TR 38.808, Release 17, 3GPP, 2021.

[9] J. Hasch, E. Topak, R. Schnabel, T. Zwick, R. Weigel, and C. Waldschmidt, "Millimeter-wave technology for automotive radar sensors in the 77 GHz frequency band," *IEEE Trans. Microw. Theory Techn.*, vol. 60, no. 3, pp. 845–860, Mar. 2012.

[10] A. M. Voicu, L. Simić, and M. Petrova, "Survey of spectrum sharing for inter-technology coexistence," *IEEE Commun. Surveys Tuts.*, vol. 21, no. 2, pp. 1112–1144, 2nd Quart., 2019.

[11] J. M. Jornet and I. F. Akyildiz, "Channel modeling and capacity analysis for electromagnetic wireless nanonetworks in the terahertz band," *IEEE Trans. Wireless Commun.*, vol. 10, no. 10, pp. 3211–3221, Oct. 2011.

[12] D. Mittleman, *Sensing With Terahertz Radiation*, vol. 85. Berlin, Germany: Springer, 2013.

[13] M. Caris et al., "Very high resolution radar at 300 GHz," in *Proc. 11th Eur. Radar Conf.*, 2014, pp. 494–496.

[14] J. Kokkoniemi, J. Lehtomäki, and M. Juntti, "A discussion on molecular absorption noise in the terahertz band," *Nano Commun. Netw.*, vol. 8, pp. 35–45, Jun. 2016.

[15] M. Giordani, M. Polese, M. Mezzavilla, S. Rangan, and M. Zorzi, "Toward 6G networks: Use cases and technologies," *IEEE Commun. Mag.*, vol. 58, no. 3, pp. 55–61, Mar. 2020.

[16] M. Polese, J. M. Jornet, T. Melodia, and M. Zorzi, "Toward end-to-end, full-stack 6G terahertz networks," *IEEE Commun. Mag.*, vol. 58, no. 11, pp. 48–54, Nov. 2020.

[17] A. F. Shehab, M. A. Elshafey, and T. A. Mahmoud, "Recurrent neural network based prediction to enhance satellite telemetry compression," in *Proc. IEEE Aerosp. Conf.*, Mar. 2020, pp. 1–11.

[18] (2020). *Radio Regulations*. [Online]. Available: http://handle.itu.int/11.1002/pub/814b0c44-en

[19] M. J. Marcus, "Harmful interference and its role in spectrum policy," *Proc. IEEE*, vol. 102, no. 3, pp. 265–269, Mar. 2014.

[20] M. M. Sohul, M. Yao, T. Yang, and J. H. Reed, "Spectrum access system for the citizen broadband radio service," *IEEE Commun. Mag.*, vol. 53, no. 7, pp. 18–25, Jul. 2015.

[21] *Amendment of the Commissions Rules With Regard to Commercial Operations in the 3550–3650 MHz Band*, document FCC 15-47 A1 GN Docket No. 12-354, Federal Communications Commission, Apr. 2015. [Online]. Available: https://docs.fcc.gov/public/attachments/FCC-15-47A1.pdf

[22] *Spectrum Management for Science in the 21st Century*, Nat. Res. Council, Nat. Acad. Press, Ottawa, ON, Canada, 2010.

[23] *Performance and Interference Criteria for Satellite Passive Remote Sensing*, document RS.2017, ITU-R, 2012. [Online]. Available: https://www.itu.int/rec/R-REC-RS.2017/en

[24] *Protection Criteria Used for Radio Astronomical Measurements*, document RA.769-2, 2003. [Online]. Available: https://www.itu.int/rec/R-REC-RA.769/en

[25] *Levels of Data Loss to Radio Astronomy Observations and Percentage-of-Time Criteria Resulting From Degradation by Interference for Frequency Bands Allocated to the Radio Astronomy Service on a Primary Basis*, document RA.1513-2, 2015. [Online]. Available: https://www.itu.int/rec/R-REC-RA.1513/en

[26] *Consideration of Sharing and Adjacent-Band Compatibility Between Passive and Active Services Above 71 GHz*, document ITU WRC-2000, Resolution 731 (Rev.WRC-19), 2019. [Online]. Available: https://www.itu.int/dms_pub/itu-r/oth/0C/0A/R0C0A00000F00149PDFE.pdf

[27] I. F. Akyildiz, C. Han, Z. Hu, S. Nie, and J. M. Jornet, "Terahertz band communication: An old problem revisited and research directions for the next decade," *IEEE Trans. Commun.*, vol. 70, no. 6, pp. 4250–4285, Jun. 2022.

[28] M. Andrello, A. Singh, N. Thawdar, and J. M. Jornet, "Dynamic beamforming algorithms for ultra-directional terahertz communication systems based on graphene-based plasmonic nano-antenna arrays," in *Proc. 52nd Asilomar Conf. Signals, Syst., Comput.*, Oct. 2018, pp. 1558–1563.

[29] *An Act to Provide for the Regulation of Interstate and Foreign Communication by Wire or Radio, and for Other Purposes*, U.S. Law, Pub. L. 73-416, 1934.

[30] M. J. Marcus, "Spectrum policy for radio spectrum access," *Proc. IEEE*, vol. 100, no. Special Centennial Issue, pp. 1685–1691, May 2012. [Online]. Available: https://ieeexplore.ieee.org/abstract/document/6170864/

[31] C. Prigent, J. R. Pardo, and W. B. Rossow, "Comparisons of the millimeter and submillimeter bands for atmospheric temperature and water vapor soundings for clear and cloudy skies," *J. Appl. Meteorol. Climatol.*, vol. 45, no. 12, pp. 1622–1633, Dec. 2006.

[32] K. B. Cooper et al., "G-band radar for humidity and cloud remote sensing," *IEEE Trans. Geosci. Remote Sens.*, vol. 59, no. 2, pp. 1106–1117, Feb. 2021.

[33] G. Skofronick-Jackson et al., "The global precipitation measurement (GPM) mission for science and society," *Bull. Amer. Meteorol. Soc.*, vol. 98, no. 8, pp. 1679–1695, 2016.

[34] D. C. Tobin et al., "Atmospheric radiation measurement site atmospheric state best estimates for atmospheric infrared sounder temperature and water vapor retrieval validation," *J. Geophys. Res., Atmos.*, vol. 111, no. D9, 2006, Art. no. D09S14.

[35] B. A. McGuire, "2018 census of interstellar, circumstellar, extragalactic, protoplanetary disk, and exoplanetary molecules," *Astrophys. J. Suppl. Ser.*, vol. 239, no. 2, p. 17, Nov. 2018.

[36] F. Combes, "Molecular gas in distant galaxies from ALMA studies," *Astron. Astrophys. Rev.*, vol. 26, no. 1, p. 5, Aug. 2018.

[37] F. Norouzian, E. G. Hoare, E. Marchetti, M. Cherniakov, and M. Gashinova, "Next generation, low-THz automotive radar—The potential for frequencies above 100 GHz," in *Proc. 20th Int. Radar Symp. (IRS)*, Jun. 2019, pp. 1–7.

[38] J. T. Richard and H. O. Everitt, "Millimeter wave and terahertz synthetic aperture radar for locating metallic scatterers embedded in scattering media," *IEEE Trans. THz Sci. Technol.*, vol. 7, no. 6, pp. 732–740, Nov. 2017.

[39] Event Horizon Telescope Collaboration, "First M87 event horizon telescope results. I. The shadow of the supermassive black hole," *Astrophys. J. Lett.*, vol. 875, no. 1, p. L1, Apr. 2019.

[40] T. R. Hunter and R. Kimberk, "Statistical topics concerning radiometer theory," in *Proc. 26th Int. Symp. Space THz Technol. (ISSTT)*, Cambridge, MA, USA, 2015, pp. 177–180. [Online]. Available: https://www.nrao.edu/meetings/isstt/papers/2015/2015000059.pdf

[41] A. J. Tetarenko et al., "Measuring fundamental jet properties with multiwavelength fast timing of the black hole X-ray binary MAXI J1820+070," *Monthly Notices Roy. Astronomical Soc.*, vol. 504, no. 3, pp. 3862–3883, Mar. 2021.

[42] J. Carpenter, D. Iono, F. Kemper, and A. Wootten, "The ALMA development program: Roadmap to 2030," 2020, *arXiv:2001.11076*.

[43] T. S. Rappaport et al., "Wireless communications and applications above 100 GHz: Opportunities and challenges for 6G and beyond," *IEEE Access*, vol. 7, pp. 78729–78757, 2019.

[44] C. Castro, R. Elschner, T. Merkle, C. Schubert, and R. Freund, "Experimental demonstrations of high-capacity THz-wireless transmission systems for beyond 5G," *IEEE Commun. Mag.*, vol. 58, no. 11, pp. 41–47, Nov. 2020.

[45] U. R. Pfeiffer, R. Jain, J. Grzyb, S. Malz, P. Hillger, and P. Rodríguez-Vízquez, "Current status of terahertz integrated circuits—From components to systems," in *Proc. IEEE BiCMOS Compound Semiconductor Integr. Circuits Technol. Symp. (BCICTS)*, Oct. 2018, pp. 1–7.

[46] N. Benvenuto, G. Cherubini, and S. Tomasin, *Algorithms for Communications Systems and Their Applications*. Hoboken, NJ, USA: Wiley, 2021.

[47] P. Banelli, S. Buzzi, G. Colavolpe, A. Modenini, F. Rusek, and A. Ugolini, "Modulation formats and waveforms for 5G networks: Who will be the heir of OFDM? An overview of alternative modulation schemes for improved spectral efficiency," *IEEE Signal Process. Mag.*, vol. 31, no. 6, pp. 80–93, Nov. 2014.

[48] G. Berardinelli, K. Pajukoski, E. Lahetkangas, R. Wichman, O. Tirkkonen, and P. Mogensen, "On the potential of OFDM enhancements as 5G waveforms," in *Proc. IEEE 79th Veh. Technol. Conf. (VTC Spring)*, May 2014, pp. 1–5.

[49] T. L. Marzetta, "Noncooperative cellular wireless with unlimited numbers of base station antennas," *IEEE Trans. Wireless Commun.*, vol. 9, no. 11, pp. 3590–3600, Nov. 2010.

[50] I. F. Akyildiz and J. M. Jornet, "Realizing ultra-massive MIMO (1024×1024) communication in the (0.06–10) terahertz band," *Nano Commun. Netw.*, vol. 8, pp. 46–54, Jun. 2016.

[51] N. Rajatheva et al., "Scoring the terabit/s goal: Broadband connectivity in 6G," 2020, *arXiv:2008.07220*.

[52] S. Palicot, Y. Corre, G. Gougeon, and J.-B. Dore. *Deliverable D1.0: Beyond-5G Wireless Tbps Scenarios and Requirements*. Accessed: Jun. 22, 2023. [Online]. Available: http://www.brave-beyond5g.com/wp-content/uploads/2018/12/BRAVE-D1.0-B5G-wireless-Tbps-Scenarios-and-Requirements-v1-1.pdf

[53] T. Kurner and T. Kawanishi, "Demonstrating 300 GHz wireless backhaul links—The ThoR approach," in *Proc. 47th Int. Conf. Infr., Millim. THz Waves (IRMMW-THz)*, Aug. 2022, p. 1.

[54] X. Xu, Y. Pan, P. P. M. Y. Lwin, and X. Liang, "3D holographic display and its data transmission requirement," in *Proc. Int. Conf. Inf. Photon. Opt. Commun.*, Oct. 2011, pp. 1–4.

[55] S. H. A. Samy, E. A. Maher, A. El-Mahdy, and F. Dressler, "Power optimization of THz band heterogeneous vehicular networks," in *Proc. IEEE Veh. Netw. Conf. (VNC)*, Nov. 2021, pp. 107–114.

[56] A. Simsek, S. Kim, and M. J. W. Rodwell, "A 140 GHz MIMO transceiver in 45 nm SOI CMOS," in *Proc. IEEE BiCMOS Compound Semiconductor Integr. Circuits Technol. Symp. (BCICTS)*, Oct. 2018, pp. 231–234.

[57] S. Kueppers, H. Cetinkaya, and N. Pohl, "A compact 120 GHz SiGe: C based 2×8 FMCW MIMO radar sensor for robot navigation in low visibility environments," in *Proc. Eur. Radar Conf. (EURAD)*, Oct. 2017, pp. 122–125.

[58] (2000). *World Radiocommunication Conference (WRC-2000) Outcomes and Documents*. [Online]. Available: http://handle.itu.int/11.1004/020.1000/4.126

[59] *Protection of the Radio Astronomy Service in Frequency Bands Shared With Other Services*, document ITU-R RA.1031-2, 2007. [Online]. Available: https://www.itu.int/rec/R-REC-RA.1031-2-200706-I/en

[60] *Typical Technical and Operational Characteristics of Earth Exploration-Satellite Service (Passive) Systems Using Allocations Between 1.4 and 275 GHz*, document RS.1861, 2010. [Online]. Available: https://www.itu.int/rec/R-REC-RS.1861/en

[61] *Typical Technical and Operating Characteristics and Frequency Bands Used by Space Research Service (Passive) Planetary Observation Systems*, document ITU-R RS.2064-0, 2014. [Online]. Available: https://www.itu.int/dms_pubrec/itu-r/rec/rs/R-REC-RS.2064-0-201412-I!!PDF-E.pdf

[62] V. Petrov, A. Pyattaev, D. Moltchanov, and Y. Koucheryavy, "Terahertz band communications: Applications, research challenges, and standardization activities," in *Proc. 8th Int. Congr. Ultra Modern Telecommun. Control Syst. Workshops (ICUMT)*, Oct. 2016, pp. 183–190.

[63] *Calculation of Free-Space Attenuation*, document P.525, 2019. [Online]. Available: https://www.itu.int/rec/R-REC-P.525/en

[64] *Attenuation by Atmospheric Gases and Related Effects*, document P.676, 2019. [Online]. Available: https://www.itu.int/rec/R-REC-P.676/en

[65] *Reference Standard Atmospheres*, document P.835, 2017. [Online]. Available: https://www.itu.int/rec/R-REC-P.835/en

[66] *The Radio Refractive Index: Its Formula and Refractivity Data*, document P.453, 2019. [Online]. Available: https://www.itu.int/rec/R-REC-P.453/en

[67] J. F. O'Hara and D. R. Grischkowsky, "Comment on the veracity of the ITU-R recommendation for atmospheric attenuation at terahertz frequencies," *IEEE Trans. THz Sci. Technol.*, vol. 8, no. 3, pp. 372–375, May 2018.

[68] *Analytical Method to Calculate Short-Term Visibility and Interference Statistics for Non-Geostationary Satellite Orbit Satellites as Seen From a Point on the Earth's Surface*, document S.1257, ITU-R, 2002. [Online]. Available: https://www.itu.int/rec/R-REC-S.1257/en

[69] *Reference Radiation Patterns for Fixed Wireless System Antennas for Use in Coordination Studies and Interference Assessment in the Frequency Range From 100 MHz to 86 GHz*, document F.699-8, 2018. [Online]. Available: https://www.itu.int/rec/R-REC-F.699/en

[70] P. Sen, D. A. Pados, S. N. Batalama, E. Einarsson, J. P. Bird, and J. M. Jornet, "The TeraNova platform: An integrated testbed for ultra-broadband wireless communications at true terahertz frequencies," *Comput. Netw.*, vol. 179, Oct. 2020, Art. no. 107370. [Online]. Available: https://www.sciencedirect.com/science/article/pii/S1389128620304473

[71] J. G. Proakis and M. Salehi, *Digital Communications*. New York, NY, USA: McGraw-Hill., 2008.

[72] X. Ge, H. Cheng, M. Guizani, and T. Han, "5G wireless backhaul networks: Challenges and research advances," *IEEE Netw.*, vol. 28, no. 6, pp. 6–11, Nov. 2014.

[73] O. P. Adare, H. Babbili, C. Madapatha, B. Makki, and T. Svensson, "Uplink power control in integrated access and backhaul networks," in *Proc.*

IEEE Int. Symp. Dyn. Spectr. Access Netw. (DySPAN), Dec. 2021, pp. 163–168.
[74] M. R. Schoeberl et al., "Overview of the EOS Aura mission," *IEEE Trans. Geosci. Remote Sens.*, vol. 44, no. 5, pp. 1066–1074, May 2006.
[75] C. L. Parkinson, "Aqua: An Earth-observing satellite mission to examine water and other climate variables," *IEEE Trans. Geosci. Remote Sens.*, vol. 41, no. 2, pp. 173–183, Feb. 2003.
[76] P. Edwards and D. Pawlak, "MetOp: The space segment for EUMETSAT's polar system," *ESA Bull.*, vol. 102, pp. 7–18, May 2000.
[77] F. Rinaldi et al., "Non-terrestrial networks in 5G & beyond: A survey," *IEEE Access*, vol. 8, pp. 165178–165200, 2020.
[78] A. J. Alqaraghuli, H. Abdellatif, and J. M. Jornet, "Performance analysis of a dual terahertz/Ka band communication system for satellite mega-constellations," in *Proc. IEEE 22nd Int. Symp. World Wireless, Mobile Multimedia Netw. (WoWMoM)*, Jun. 2021, pp. 316–322.
[79] S. Wan, J. Hu, C. Chen, A. Jolfaei, S. Mumtaz, and Q. Pei, "Fair-hierarchical scheduling for diversified services in space, air and ground for 6G-dense Internet of Things," *IEEE Trans. Netw. Sci. Eng.*, vol. 8, no. 4, pp. 2837–2848, Oct. 2021.
[80] L. Bertizzolo et al., "Live and let live: Flying UAVs without affecting terrestrial UEs," in *Proc. 21st Int. Workshop Mobile Comput. Syst. Appl.* Austin, TX, USA: Association for Computing Machinery, Mar. 2020, pp. 21–26.
[81] A. Williams et al., "A report to ESO council on the impact of satellite constellations," 2021, *arXiv:2108.03999*.
[82] C. A. Balanis, *Antenna Theory: Analysis and Design*. Hoboken, NJ, USA: Wiley, 2016.
[83] V. Jamnejad, J. Huang, B. Levitt, T. Pham, and R. Cesarone, "Array antennas for JPL/NASA deep space network," in *Proc. IEEE Proc. Aerosp. Conf.*, vol. 2, Mar. 2002, p. 2.
[84] L. Zhang, M. Xiao, G. Wu, M. Alam, Y. Liang, and S. Li, "A survey of advanced techniques for spectrum sharing in 5G networks," *IEEE Wireless Commun.*, vol. 24, no. 5, pp. 44–51, Oct. 2017.
[85] F. Hu, B. Chen, and K. Zhu, "Full spectrum sharing in cognitive radio networks toward 5G: A survey," *IEEE Access*, vol. 6, pp. 15754–15776, 2018.
[86] Y. Han, E. Ekici, H. Kremo, and O. Altintas, "Spectrum sharing methods for the coexistence of multiple RF systems: A survey," *Ad Hoc Netw.*, vol. 53, pp. 53–78, Dec. 2016. [Online]. Available: https://www.sciencedirect.com/science/article/pii/S1570870516302153
[87] M. Fitch, M. Nekovee, S. Kawade, K. Briggs, and R. MacKenzie, "Wireless service provision in TV white space with cognitive radio technology: A telecom operator's perspective and experience," *IEEE Commun. Mag.*, vol. 49, no. 3, pp. 64–73, Mar. 2011.
[88] Z. Zhang et al., "6G wireless networks: Vision, requirements, architecture, and key technologies," *IEEE Veh. Technol. Mag.*, vol. 14, no. 3, pp. 28–41, Sep. 2019.
[89] L. Dai, B. Wang, Z. Ding, Z. Wang, S. Chen, and L. Hanzo, "A survey of non-orthogonal multiple access for 5G," *IEEE Commun. Surveys Tuts.*, vol. 20, no. 3, pp. 2294–2323, 3rd Quart., 2018.
[90] L. Zhang, Y.-C. Liang, and M. Xiao, "Spectrum sharing for Internet of Things: A survey," *IEEE Wireless Commun.*, vol. 26, no. 3, pp. 132–139, Jun. 2019.
[91] Y. R. Ramadan, H. Minn, and Y. Dai, "A new paradigm for spectrum sharing between cellular wireless communications and radio astronomy systems," *IEEE Trans. Commun.*, vol. 65, no. 9, pp. 3985–3999, Sep. 2017.
[92] Y. Cho, H.-K. Kim, M. Nekovee, and H.-S. Jo, "Coexistence of 5G with satellite services in the millimeter-wave band," *IEEE Access*, vol. 8, pp. 163618–163636, 2020.
[93] M. Marcus, X. C. Roman, and J. Jornet, "Millimeter-wave propagation: Spectrum management implications—An update for >100 GHz [speaker's corner]," *IEEE Microw. Mag.*, vol. 24, no. 1, pp. 91–94, Jan. 2023.
[94] I. Khalifa and R. Vaughan, "Geometric design of pyramidal antenna arrays for hemispherical scan coverage," *IEEE Trans. Antennas Propag.*, vol. 55, no. 2, pp. 468–471, Feb. 2007.
[95] A. F. Molisch et al., "Hybrid beamforming for massive MIMO: A survey," *IEEE Commun. Mag.*, vol. 55, no. 9, pp. 134–141, Sep. 2017.
[96] S. W. Varade and K. D. Kulat, "Robust algorithms for DOA estimation and adaptive beamforming for smart antenna application," in *Proc. 2nd Int. Conf. Emerg. Trends Eng. Technol.*, 2009, pp. 1195–1200.
[97] M. D. Renzo et al., "Smart radio environments empowered by reconfigurable AI meta-surfaces: An idea whose time has come," *EURASIP J. Wireless Commun. Netw.*, vol. 2019, no. 1, pp. 1–20, Dec. 2019.
[98] N. M. Monroe, G. C. Doqiamis, R. Stingel, P. Myers, X. Chen, and R. Han, "Electronic THz pencil beam forming and 2D steering for high angular-resolution operation: A 98×98-unit 265 GHz CMOS reflectarray with in-unit digital beam shaping and squint correction," in *IEEE Int. Solid-State Circuits Conf. (ISSCC) Dig. Tech. Papers*, vol. 65, Feb. 2022, pp. 1–3.
[99] M. J. W. Rodwell, "100–340 GHz spatially multiplexed communications: IC, transceiver, and link design," in *Proc. IEEE 20th Int. Workshop Signal Process. Adv. Wireless Commun. (SPAWC)*, Jul. 2019, pp. 1–5.
[100] A. Singh, A. J. Alqaraghuli, and J. M. Jornet, "Wavefront engineering at terahertz frequencies through intelligent reflecting surfaces," in *Proc. IEEE 23rd Int. Workshop Signal Process. Adv. Wireless Commun. (SPAWC)*, Jul. 2022, pp. 1–5.
[101] C. Liaskos, S. Nie, A. Tsioliaridou, A. Pitsillides, S. Ioannidis, and I. Akyildiz, "A novel communication paradigm for high capacity and security via programmable indoor wireless environments in next generation wireless systems," *Ad Hoc Netw.*, vol. 87, pp. 1–16, May 2019.
[102] S. Liu et al., "A review of anomalous refractive and reflective metasurfaces," *Nanotechnol. Precis. Eng.*, vol. 5, no. 2, Jun. 2022, Art. no. 025001.
[103] Z. Shaikhanov, S. Badran, J. M. Jornet, D. M. Mittleman, and E. W. Knightly, "Remotely positioned metasurface-drone attack," in *Proc. 24th Int. Workshop Mobile Comput. Syst. Appl.*, Feb. 2023, pp. 110–116.
[104] S. Sun, T. S. Rappaport, R. W. Heath Jr., A. Nix, and S. Rangan, "MIMO for millimeter-wave wireless communications: Beamforming, spatial multiplexing, or both?" *IEEE Commun. Mag.*, vol. 52, no. 12, pp. 110–121, Dec. 2014.
[105] A. R. Vilenskiy, E. Galesloot, Y. Zhang, A. Bart Smolders, and M. V. Ivashina, "Quasi-optical beamforming network for millimeter-wave electronically scanned array antennas with 1-bit phase resolution," in *Proc. 15th Eur. Conf. Antennas Propag. (EuCAP)*, Mar. 2021, pp. 1–5.
[106] P. Chen and A. Alù, "THz beamforming using graphene-based devices," in *Proc. IEEE Radio Wireless Symp.*, Jan. 2013, pp. 55–57.
[107] J. M. Jornet and I. F. Akyildiz, "Graphene-based plasmonic nano-transceiver for terahertz band communication," in *Proc. 8th Eur. Conf. Antennas Propag. (EuCAP)*, Apr. 2014, pp. 492–496.
[108] J. Crabb, X. Cantos-Roman, J. M. Jornet, and G. R. Aizin, "Hydrodynamic theory of the Dyakonov–Shur instability in graphene transistors," *Phys. Rev. B, Condens. Matter*, vol. 104, no. 15, Oct. 2021, Art. no. 155440.
[109] P. K. Singh, G. Aizin, N. Thawdar, M. Medley, and J. M. Jornet, "Graphene-based plasmonic phase modulator for terahertz-band communication," in *Proc. 10th Eur. Conf. Antennas Propag. (EuCAP)*, Apr. 2016, pp. 1–5.
[110] J. Crabb, X. Cantos-Roman, G. R. Aizin, and J. M. Jornet, "Amplitude and frequency modulation with an on-chip graphene-based plasmonic terahertz nanogenerator," *IEEE Trans. Nanotechnol.*, vol. 21, pp. 539–546, 2022.
[111] J. M. Jornet and I. F. Akyildiz, "Graphene-based plasmonic nano-antenna for terahertz band communication in nanonetworks," *IEEE J. Sel. Areas Commun.*, vol. 31, no. 12, pp. 685–694, Dec. 2013.
[112] A. Singh, M. Andrello, N. Thawdar, and J. M. Jornet, "Design and operation of a graphene-based plasmonic nano-antenna array for communication in the terahertz band," *IEEE J. Sel. Areas Commun.*, vol. 38, no. 9, pp. 2104–2117, Sep. 2020.
[113] M. H. Dahri, M. H. Jamaluddin, M. Khalily, M. I. Abbasi, R. Selvaraju, and M. R. Kamarudin, "Polarization diversity and adaptive beamsteering for 5G reflectarrays: A review," *IEEE Access*, vol. 6, pp. 19451–19464, 2018.
[114] A. Singh, M. Andrello, E. Einarsson, N. Thawdarl, and J. M. Jornet, "A hybrid intelligent reflecting surface with graphene-based control elements for THz communications," in *Proc. IEEE 21st Int. Workshop Signal Process. Adv. Wireless Commun. (SPAWC)*, May 2020, pp. 1–5.
[115] B. A. Munk, *Frequency Selective Surfaces: Theory and Design*. Hoboken, NJ, USA: Wiley, 2005.
[116] M. A. Al-Joumayly and N. Behdad, "Wideband planar microwave lenses using sub-wavelength spatial phase shifters," *IEEE Trans. Antennas Propag.*, vol. 59, no. 12, pp. 4542–4552, Dec. 2011.
[117] M. Li, M. A. Al-Joumayly, and N. Behdad, "Broadband true-time-delay microwave lenses based on miniaturized element frequency selective surfaces," *IEEE Trans. Antennas Propag.*, vol. 61, no. 3, pp. 1166–1179, Mar. 2013.
[118] U. Nissanov, G. Singh, and N. Kumar, "High gain microstrip array antenna with SIW and FSS for beyond 5G at THz band," *Optik*, vol. 236, Jun. 2021, Art. no. 166568.
[119] B. Zhang, J. M. Jornet, I. F. Akyildiz, and Z. P. Wu, "Mutual coupling reduction for ultra-dense multi-band plasmonic nano-antenna arrays using graphene-based frequency selective surface," *IEEE Access*, vol. 7, pp. 33214–33225, 2019.
[120] S. Venkatesh, X. Lu, H. Saeidi, and K. Sengupta, "A high-speed programmable and scalable terahertz holographic metasurface based on tiled CMOS chips," *Nature Electron.*, vol. 3, pp. 785–793, Dec. 2020.
[121] P. A. Fridman and W. A. Baan, "RFImitigation methods in radio astronomy," *Astron. Astrophys.*, vol. 378, no. 1, pp. 327–344, Oct. 2001, doi: 10.1051/0004-6361:20011166.
[122] J. E. Balling, S. S. Søbjærg, S. S. Kristensen, and N. Skou, "RFI detected by kurtosis and polarimetry: Performance comparison based on airborne campaign data," in *Proc. 12th Spec. Meeting Microw. Radiometry Remote Sens. Environ. (MicroRad)*, Mar. 2012, pp. 1–4.
[123] D. Bradley, J. M. Morris, T. Adali, J. T. Johnson, and M. Aksoy, "On the detection of RFI using the complex signal kurtosis in microwave radiometry," in *Proc. 13th Spec. Meeting Microw. Radiometry Remote Sens. Environ. (MicroRad)*, Mar. 2014, pp. 33–38.
[124] J. R. Piepmeier et al., "Radio-frequency interference mitigation for the soil moisture active passive microwave radiometer," *IEEE Trans. Geosci. Remote Sens.*, vol. 52, no. 1, pp. 761–775, Jan. 2014.
[125] J. R. Piepmeier et al., "SMAP L-band microwave radiometer: Instrument design and first year on orbit," *IEEE Trans. Geosci. Remote Sens.*, vol. 55, no. 4, pp. 1954–1966, Apr. 2017.
[126] J. T. Johnson, P. N. Mohammed, J. R. Piepmeier, A. Bringer, and M. Aksoy, "Soil moisture active passive (SMAP) microwave radiometer radio-frequency interference (RFI) mitigation: Algorithm updates and performance assessment," in *Proc. IEEE Int. Geosci. Remote Sens. Symp. (IGARSS)*, Jul. 2016, pp. 123–124.
[127] J. Querol, A. Alonso-Arroyo, R. Onrubia, D. Pascual, and A. Camps, "Assessment of back-end RFI mitigation techniques in passive remote sensing," in *Proc. IEEE Int. Geosci. Remote Sens. Symp. (IGARSS)*, Jul. 2015, pp. 4746–4749.
[128] L. W. Peck and D. M. Fenech, "SERPent: Automated reduction and RFI-mitigation software for e-MERLIN," *Astron. Comput.*, vol. 2, pp. 54–66,

Aug. 2013. [Online]. Available: https://www.sciencedirect.com/science/article/pii/S2213133713000255
[129] Z.-S. Zhang et al., "First SETI observations with China's five-hundred-meter aperture spherical radio telescope (FAST)," *Astrophys. J.*, vol. 891, no. 2, p. 174, Mar. 2020, doi: 10.3847/1538-4357/ab7376.
[130] R. V. van Nieuwpoort, "Towards exascale real-time RFI mitigation," in *Proc. Radio Freq. Interference (RFI)*, Oct. 2016, pp. 69–74.
[131] V. Ariyarathna, A. Madanayake, and J. M. Jornet, "Real-time digital baseband system for ultra-broadband THz communication," in *Proc. 45th Int. Conf. Infr., Millim., THz Waves (IRMMW-THz)*, Nov. 2020, pp. 1–2.
[132] R. Selina, U. Rau, R. Hiriart, and A. Erickson. (2020). *RFI Mitigation in the ngVLA System Architecture ngVLA Memo# 71*. [Online]. Available: https://library.nrao.edu/public/memos/ngvla/NGVLA_71.pdf
[133] D. M. Le Vine, J. T. Johnson, and J. Piepmeier, "RFI and remote sensing of the Earth from space," in *Proc. Radio Freq. Interference (RFI)*, Oct. 2016, pp. 49–54.
[134] C. Han, L. Yan, and J. Yuan, "Hybrid beamforming for terahertz wireless communications: Challenges, architectures, and open problems," *IEEE Wireless Commun.*, vol. 28, no. 4, pp. 198–204, Aug. 2021.
[135] K. S. Zigangirov, *Theory of Code Division Multiple Access Communication*, vol. 6. Hoboken, NJ, USA: Wiley, 2004.
[136] C. Bosso, P. Sen, X. Cantos-Roman, C. Parisi, N. Thawdar, and J. M. Jornet, "Ultrabroadband spread spectrum techniques for secure dynamic spectrum sharing above 100 GHz between active and passive users," in *Proc. IEEE Int. Symp. Dyn. Spectr. Access Netw. (DySPAN)*, Dec. 2021, pp. 45–52.
[137] P. Sen, H. Pandey, and J. M. Jornet, "Ultra-broadband chirp spread spectrum communication in the terahertz band," *Proc. SPIE*, vol. 11390, pp. 7–18, May 2020.
[138] S. Aliaga, A. J. Alqaraghuli, and J. M. Jornet, "Joint terahertz communication and atmospheric sensing in low Earth orbit satellite networks: Physical layer design," in *Proc. IEEE 23rd Int. Symp. World Wireless, Mobile Multimedia Netw. (WoWMoM)*, Jun. 2022, pp. 457–463.
[139] A. Grami, *Introduction to Digital Communications*. New York, NY, USA: Academic, 2015.
[140] P. Luethi et al., "Gram-Schmidt-based QR decomposition for MIMO detection: VLSI implementation and comparison," in *Proc. IEEE Asia Pacific Conf. Circuits Syst. (APCCAS)*, Nov. 2008, pp. 830–833.
[141] C. Shi and G. Li, "Coordinated blanking for 5G millimeter-wave networks spectrum sharing," in *Proc. IEEE 83rd Veh. Technol. Conf. (VTC Spring)*, May 2016, pp. 1–5.
[142] M. Polese et al., "Dynamic spectrum sharing between active and passive users above 100 GHz," *Commun. Eng.*, vol. 1, no. 1, pp. 1–9, May 2022.
[143] B. Peng, K. Guan, A. Kuter, S. Rey, M. Patzold, and T. Kuerner, "Channel modeling and system concepts for future terahertz communications: Getting ready for advances beyond 5G," *IEEE Veh. Technol. Mag.*, vol. 15, no. 2, pp. 136–143, Jun. 2020.
[144] A. B. Kihero, M. S. J. Solaija, A. Yazar, and H. Arslan, "Inter-numerology interference analysis for 5G and beyond," in *Proc. IEEE Globecom Workshops (GC Wkshps)*, Dec. 2018, pp. 1–6.
[145] N. Patriciello, S. Lagen, L. Giupponi, and B. Bojovic, "5G new radio numerologies and their impact on the end-to-end latency," in *Proc. IEEE 23rd Int. Workshop Comput. Aided Model. Design Commun. Links Netw. (CAMAD)*, Sep. 2018, pp. 1–6.
[146] M. Polese, L. Bonati, S. D'Oro, S. Basagni, and T. Melodia, "Understanding O-RAN: Architecture, interfaces, algorithms, security, and research challenges," *IEEE Commun. Surveys Tuts.*, vol. 25, no. 2, pp. 1376–1411, 2nd Quart., 2023.
[147] R. J. Baxley and R. S. Thompson. *Deep Learning Collaborative Radios—Team Zylinium Phase 3, AFRL-RI-RS-TR-2020-158*. Accessed: Jun. 22, 2023. [Online]. Available: https://apps.dtic.mil/sti/pdfs/AD1107855.pdf
[148] R. J. Baxley and R. S. Thompson, "Team zylinium DARPA spectrum collaboration challenge radio design and implementation," in *Proc. IEEE Int. Symp. Dyn. Spectr. Access Netw. (DySPAN)*, Nov. 2019, pp. 1–6.
[149] PAWR Project Office (PPO). *New $2.7M PAWR Project Funded by the U.S. Department of Defense Will Test AI-Driven Spectrum Sharing Optimization In a 5G-NR Network*. Accessed: Jun. 22, 2023. [Online]. Available: https://advancedwireless.org/new-2-7m-pawr-project-funded-by-the-us-department-of-defense-will-test-ai-driven-spectrum-sharing-optimization-in-a-5g-nr-network/
[150] E. Eichen, "Real-time geographical spectrum sharing by 5G networks and Earth exploration satellite services," in *Proc. IEEE Int. Symp. Dyn. Spectr. Access Netw. (DySPAN)*, Nov. 2019, pp. 1–2.
[151] L. Bonati et al., "Colosseum: Large-scale wireless experimentation through hardware-in-the-loop network emulation," in *Proc. IEEE Int. Symp. Dyn. Spectr. Access Netw. (DySPAN)*, Dec. 2021, pp. 105–113.

ABOUT THE AUTHORS

Michele Polese (Member, IEEE) received the Ph.D. degree from the Department of Information Engineering, University of Padua, Padua, Italy, in 2020, under the supervision of Michele Zorzi.

He was an Adjunct Professor and a Postdoctoral Researcher with the University of Padua in 2019 and 2020, and a part-time Lecturer with Northeastern University, Boston, MA, USA, in fall 2020 and 2021. During his Ph.D. degree, he visited New York University (NYU), New York, NY, USA; AT&T Labs, Bedminster, NJ, USA; and Northeastern University. He collaborated with several academic and industrial research partners. He has been a Principal Research Scientist with Northeastern University since March 2020. His research interests are in the analysis and development of protocols and architectures for future generations of cellular networks (5G and beyond), in particular for millimeter-wave communication, and in the performance evaluation of complex networks.

Dr. Polese was awarded several best paper awards. He has served as the TPC Co-Chair of Workshop on ns-3 (WNS3) from 2021 to 2022. He is also serving as an Associate Technical Editor for the *IEEE Communications Magazine*.

Xavier Cantos-Roman (Graduate Student Member, IEEE) received the B.S. degree in telecommunications technologies and services engineering from the Universitat Politécnica de Catalunya, Barcelona, Spain, in 2019. He is currently pursuing the Ph.D. degree with the Ultra-Broadband Nanonetworking Laboratory, Northeastern University, Boston, MA, USA, under the guidance of Dr. Josep Miquel Jornet.

He is currently a member of the Ultra-Broadband Nanonetworking Laboratory, Northeastern University. His research interests include the modeling and simulation of THz plasmonic devices, the study of mmWave and THz signals propagation, and the design and experimental demonstration of joint communication and sensing systems at sub-THz frequencies.

Arjun Singh (Member, IEEE) received the B.S. (summa cum laude) and M.S. degrees in electrical engineering from the University at Buffalo, The State University of New York, Buffalo, NY, USA, in 2016 and 2018, respectively, and the Ph.D. degree in electrical engineering from Northeastern University, Boston, MA, USA, under the guidance of Dr. Josep Miquel Jornet, in December 2021.

He was a member of the Ultra-Broadband Nanonetworking Laboratory, Northeastern University. Since 2022, he has been an Assistant Professor with the Department of Engineering, State University of New York Polytechnic Institute, Utica, NY, USA. His research interests include realizing terahertz-band wireless communications, dynamic spectrum sharing, space networks, wavefront engineering, graphene plasmonics, and intelligent reflecting surfaces. In these areas, he has coauthored several publications in leading journals and one U.S. patent.

Dr. Singh is also serving as the Media Chair of the IEEE RCC Special Interest Group on Terahertz Communications and a Reviewer for reputed journals, including *IEEE Communications Magazine*.

Michael J. Marcus (Life Fellow, IEEE) received the S.B. and Sc.D. degrees in electrical engineering from the Massachusetts Institute of Technology (MIT), Cambridge, MA, USA, in 1968 and 1972, respectively.

He retired from the Federal Communications Commission in 2004 after nearly 25 years in senior spectrum policy positions. While at FCC, he proposed and directed the policy developments that resulted in the bands used by Wi-Fi, Bluetooth, and licensed and unlicensed millimeter-wave systems above 59 GHz. He was an Exchange Visitor from FCC to the Japanese spectrum regulator (now MIC) and has been a Consultant to the European Commission and the Singapore regulator (now IMDA). He is currently the Director of Marcus Spectrum Solutions, Cabin John, MD, USA, and an Adjunct Professor with the Department of Electrical and Computer Engineering, Northeastern University, Boston, MA, USA.

Dr. Marcus was awarded the IEEE ComSoc Award for Public Service in the Field of Telecommunications in 2013 "for pioneering spectrum policy initiatives that created modern unlicensed spectrum bands for applications that have changed our world." From 2012 to 2013, he was the Chair of the IEEE-USA Committee on Communication Policy and is now its Vice-Chair for spectrum policy.

Thomas J. Maccarone was born in Haverhill, MA, USA, in August 1974. He received the B.S. degree in physics from the California Institute of Technology, Pasadena, CA, USA, in 1996, and the M.S. and M.Phil. degrees and the Ph.D. degree in astronomy from Yale University, New Haven, CT, USA, in 1999 and 2001.

After postdoctoral fellowships at the Scuola Internazionale Superiore di Studi Avanzati, Trieste, Italy, and the University of Amsterdam, Amsterdam, The Netherlands, he was a Lecturer and then a Reader with the School of Physics of Astronomy, University of Southampton, Southampton, U.K., from 2005 to 2012. In 2013, he moved to Texas Tech University, Lubbock, TX, USA, as an Associate Professor at the Department of Physics to help start the university's astrophysics research program and is currently a Presidential Excellence in Research Professor at its Department of Physics and Astronomy. He has been heavily involved in efforts to plan the science cases for a wide range of new observational facilities. His main area of research is understanding the physics of accretion and radio jet production in X-ray binaries and the processes of binary formation and evolution for these systems.

Dr. Maccarone serves on advisory panels to the National Radio Astronomy Observatory and the Executive Committee of the High Energy Astrophysics Division of the American Astronomical Society.

Tommaso Melodia (Fellow, IEEE) received the Ph.D. degree in electrical and computer engineering from the Georgia Institute of Technology, Atlanta, GA, USA, in 2007.

He is currently the William Lincoln Smith Chair Professor with the Department of Electrical and Computer Engineering, Northeastern University, Boston, MA, USA. He is also the Founding Director of the Institute for the Wireless Internet of Things, Northeastern University. He is also the Director of Research for the Platforms for Advanced Wireless Research (PAWR) Project Office, a $100M public-private partnership to establish four city-scale platforms for wireless research to advance the U.S. wireless ecosystem in years to come. His research on the Internet of Things and wireless networked systems has been funded by the National Science Foundation, the Air Force Research Laboratory the Office of Naval Research, Defense Advanced Research Projects Agency (DARPA), and the Army Research Laboratory.

Prof. Melodia is a Senior Member of the ACM. He was a recipient of the NSF CAREER Award. He has served as an Associate Editor for IEEE TRANSACTIONS ON WIRELESS COMMUNICATIONS, IEEE TRANSACTIONS ON MOBILE COMPUTING, and *Computer Networks* (Elsevier), among others. He has served as the Technical Program Committee Chair of IEEE International Conference on Computer Communications (Infocom) 2018 and the General Chair of IEEE Sensing, Communication, and Networking (SECON) 2019, ACM Nanoscale Computing and Communication (Nanocom) 2019, and ACM International Conference on Underwater Networks and Systems (WUWNet) 2014.

Josep Miquel Jornet (Senior Member, IEEE) received the Engineering degree in telecommunication engineering and the M.Sc. degree in information and communication technologies from the Universitat Politécnica de Catalunya, Barcelona, Spain, in 2008, and the Ph.D. degree in electrical and computer engineering from the Georgia Institute of Technology, Atlanta, GA, USA, in August 2013.

He is currently an Associate Professor with the Department of Electrical and Computer Engineering, the Director of the Ultra-broadband Nanonetworking (UN) Laboratory, and a member of the Institute for the Wireless Internet of Things and the SMART Center, Northeastern University (NU), Boston, MA, USA. His work received more than 13 800 citations (H-index of 54 as of December 2022). His core research is in terahertz communications, in addition to wireless nano-bio-communication networks and the Internet of Nano-Things. In these areas, he has coauthored more than 220 peer-reviewed scientific publications, including one book and five U.S. patents.

Dr. Jornet was a recipient of multiple awards from IEEE and ACM, and four best paper awards. He is serving as the Lead PI on multiple grants from U.S. federal agencies, including the National Science Foundation, the Air Force Office of Scientific Research, and the Air Force Research Laboratory, as well as the industry. He is also the Editor-in-Chief of the *Nano Communication Networks* (Elsevier) journal and an Editor of IEEE TRANSACTIONS ON COMMUNICATIONS. He is an IEEE ComSoc Distinguished Lecturer (Class of 2022-2023).